



1 **Regional and seasonal radiative forcing by perturbations to**
2 **aerosol and ozone precursor emissions**

3 **Nicolas Bellouin¹, Laura Baker¹, Øivind Hodnebrog², Dirk Olivie³, Ribu**
4 **Cherian⁴, Claire Macintosh¹, Bjørn Samset², Anna Esteve^{1,*}, Borgar Aamaas²,**
5 **Johannes Quaas⁴, and Gunnar Myhre².**

6 [1]{Department of Meteorology, University of Reading, Reading, United Kingdom}

7 [2]{Center for International Climate and Environmental Research – Oslo (CICERO), Oslo,
8 Norway}

9 [3]{Norwegian Meteorological Institute, Oslo, Norway}

10 [4]{Universität Leipzig, Leipzig, Germany}

11 [*]{now at: University of Valencia, Valencia, Spain}

12 Correspondence to: N. Bellouin (n.bellouin@reading.ac.uk)

13



1 **Abstract**

2 Dedicated model simulations by four general circulation and chemistry-transport models are
3 used to establish a matrix of specific radiative forcing, defined as the radiative forcing per unit
4 change in mass emitted, as a function of the near-term climate forcer emitted, its source
5 region, and the season of emission. Emissions of eight near-term climate forcers are reduced:
6 sulphur dioxide, the precursor to sulphate aerosols; black carbon aerosols; organic carbon
7 aerosols; ammonia, a precursor to nitrate aerosols; methane; and nitrogen oxides, carbon
8 monoxide, and volatile organic compounds, the precursors to ozone and to secondary organic
9 aerosols. The focus is on two source regions, Europe and East Asia, but the shipping sector
10 and global averages are also included. Emission reductions are applied over two time periods:
11 May-Oct and Nov-Apr. Models generally agree on the sign and ranking of specific radiative
12 forcing for different emitted species, but disagree quantitatively. Black carbon aerosols,
13 methane, and carbon monoxide exert positive specific radiative forcings. Black carbon exerts
14 the strongest specific radiative forcing, even after accounting for rapid adjustments from the
15 semi-direct effect, and is most efficient in local summer. However, although methane and
16 carbon monoxide are less efficient in a specific sense, the potential for decreasing the mass
17 emitted is larger. Organic carbon aerosols, sulphur dioxide, ammonia, and emissions by the
18 shipping sector exert negative specific radiative forcings, with local summer emission
19 changes being again more efficient. Ammonia is notable for its weak specific radiative
20 forcing. For aerosols, specific radiative forcing exerted by European emissions is stronger
21 than for East Asia, because the European baseline is less polluted. Radiative forcing of
22 European and East Asian emission reductions is mainly exerted in the mid-latitudes of the
23 Northern Hemisphere, but atmospheric transport yields sizeable radiative forcings in
24 neighbouring regions, such as the Arctic. Models disagree on the sign of the net radiative
25 forcing exerted by reductions in the emissions of nitrogen oxides and volatile organic
26 compounds, because those reductions trigger complex changes in the oxidising capacity of the
27 atmosphere, translating into radiative forcings by aerosols, methane, and ozone of different
28 signs. The response of nitrate aerosols to nitrogen oxide reductions is particularly important in
29 determining the sign of the corresponding radiative forcing. Model diversity comes from
30 different modelled lifetimes, different unperturbed baselines, and different numbers of species
31 and radiative forcing mechanisms represented. The strength of the aerosol-chemistry coupling



1 is also diverse, translating into aerosol responses to perturbations of ozone precursors of
2 different magnitudes.

3

4 Keywords: Radiative forcing; near-term climate forcers; Aerosols; Methane; Ozone

5

6 **1 Introduction**

7 Human activities have profoundly modified the composition of the atmosphere by increasing
8 the concentrations of long-lived greenhouse gases, such as carbon dioxide or
9 chlorofluorocarbons, and medium- to short-lived species, such as methane, tropospheric
10 ozone and aerosols. Once in the atmosphere, those species perturb the energy budget of the
11 Earth, exerting a radiative forcing (RF) of the climate system by various mechanisms which
12 depend on the species. Greenhouse gases, including methane, and ozone absorb longwave
13 radiation. Ozone is also an important absorber of shortwave radiation, mainly at ultraviolet
14 wavelengths. Aerosols scatter and absorb shortwave and, for larger particles, longwave
15 radiation: this mechanism is herein called aerosol-radiation interactions and denoted *ari*,
16 following Boucher et al. (2013). Changes in aerosol concentrations also translate in aerosol-
17 cloud interactions (*aci*) through changes in the number of cloud condensation nuclei,
18 modifying the radiative properties and life cycle of clouds. Aerosols that absorb shortwave
19 radiation, such as mineral dust and black carbon aerosols, also change the surface albedo
20 when depositing on snow or ice.

21 Figure 1 gives a simplified view of the tropospheric chemistry of ozone and its precursors. At
22 its heart are two equilibria: between nitrogen oxide (NO) and nitrous oxide (NO₂), and
23 between the hydroxyl (OH) and hydroperoxyl (HO₂) radicals. Photolysis of NO₂ is a source of
24 atomic oxygen which combines with molecular oxygen (O₂) to form ozone. Ozone, in turn,
25 undergoes photolysis to provide the principal source of OH. OH is converted into HO₂ during
26 oxidation of carbon monoxide (CO), CH₄, and other hydrocarbons. Then the reaction between
27 HO₂ and NO regenerates both NO₂ and OH. Nitric acid (HNO₃) and hydrogen peroxide
28 (H₂O₂) are sinks of NO/NO₂ and HO₂, respectively. Tropospheric ozone is removed by dry
29 deposition. The lifetime of CH₄ is primarily determined by the abundance of OH, but volatile
30 organic compounds (VOCs) are also important. When the concentrations of CH₄, CO, and
31 VOCs increase, the limiting factor in the recycling of OH is the concentration of NO. VOCs



1 therefore control the rate of ozone production where NO_x concentrations are not a limiting
2 factor. In addition, VOCs perturb the distribution of CH_4 by modifying OH concentrations.
3 Finally, OH, O_3 , HO_2 , and H_2O_2 are also involved in the dry and in-cloud oxidation of SO_2 ,
4 the gaseous precursor to sulphate aerosol. Those tight interactions between species add
5 components to the RF caused by feedbacks of one species onto another: for example, changes
6 in methane concentrations trigger changes in tropospheric ozone, which exerts its own RF,
7 called primary-mode ozone RF (Prather, 1996). Shindell et al. (2009) found sizeable impacts
8 of nitrogen oxides (NO_x), CO, and CH_4 emissions on aerosol formation in global simulations
9 of atmospheric chemistry with the Goddard Institute for Space Studies (GISS) model. The
10 crucial link in those chemical feedbacks is OH, which in spite of its very short lifetime plays
11 an important role in both the atmospheric chemistry of ozone and the oxidation of aerosol
12 gaseous precursors.

13 The fifth assessment report of the Intergovernmental Panel on Climate Change (IPCC)
14 formalised two RF concepts: the stratospherically-adjusted and effective RF (Boucher et al.,
15 2013; Myhre et al., 2013a). In the first definition, surface and tropospheric conditions are held
16 fixed to their unperturbed state, but stratospheric temperatures are allowed to adjust. In
17 contrast, effective RF (ERF) also includes rapid adjustments to the tropospheric state. Those
18 rapid adjustments occur on shorter timescales than deep ocean and sea ice changes and
19 include such processes as the change in cloud cover that follows the local atmospheric
20 warming caused by aerosol absorption of shortwave radiation, the change in cloud cover due
21 to aerosol-driven changes in precipitation efficiency, the increased spring melting that follows
22 black carbon deposition on snow, or the change in cloud cover that immediately follows
23 changes in thermodynamic profiles in response to an increase in carbon dioxide
24 concentrations. Because ERF includes rapid adjustments, it is a better indicator of the
25 eventual surface temperature response than RF. It has however recently been suggested that
26 an additional efficacy, acting not on the RF but on temperature change itself, is needed to
27 account for differences in global patterns of ERF, whereby forcing agents located in the
28 Northern Hemisphere cause more rapid land surface temperature responses (Shindell, 2014).
29 Both stratospherically-adjusted and effective RF exclude the radiative impact of large-scale
30 changes in sea surface temperatures, which are part of the climate response.



1 Climate metrics such as Global Warming Potential and Global Temperature Change Potential
2 (e.g. Shine et al., 2005) have been developed to compare the climate impact of the emissions
3 of different species, trying to account for both the radiative forcing efficiency of the species
4 and their lifetime. Emission-based climate metrics allow the exploration of future mitigation
5 options where the basket of species emitted by a given sector of activity changes in response
6 to policies and technological advances. Those metrics require the knowledge of
7 stratospherically-adjusted RF exerted per change in unit mass emission rate, hereafter called
8 specific RF (SRF) and given in $\text{mW m}^{-2} (\text{Tg yr}^{-1})^{-1}$.

9 In the past, the available literature has been used in a rather ad-hoc way to quantify SRF.
10 Table 1 summarises estimates from five previous multi-model studies. Bond et al. (2013)
11 assessed black carbon (BC) emissions and RF over the period 1750—2005 based on multi-
12 model estimates scaled to remove biases in absorption aerosol optical depth against present-
13 day observations. Myhre et al. (2013b) conducted a multi-model inter-comparison of RFari
14 over the period 1850—2000 by the second phase of the AeroCom (Aerosol Comparisons
15 between Observations and Models) initiative. Shindell et al. (2013) and Stevenson
16 et al. (2013) document multi-model inter-comparisons of aerosol and ozone RF, respectively,
17 over the period 1850—2000 by the Atmospheric Chemistry and Climate Model Inter-
18 comparison Project (ACCMIP, Lamarque et al., 2013). Finally, Yu et al. (2013) report results
19 of a multi-model inter-comparison of RF due to 20% reductions in the emissions of 4 regions
20 as part of the Hemispheric Transport of Air Pollution (HTAP) project. Table 1 also shows
21 results for the present study to allow for an easy comparison: results are discussed in Sect. 4.

22 All studies agree on the sign of the SRF of individual species. All near-term climate forcers
23 (NTCFs) exert positive SRFs, which lead to a gain in energy for the climate system when
24 emissions are increased, except for sulphate, organic carbon (OC), and nitrate aerosols, and
25 nitrogen oxide gases, which exert negative SRFs. According to those studies, BC exerts the
26 strongest SRF of all NTCFs, in absolute values. Compared to other aerosol species, its SRF is
27 an order of magnitude larger. Among ozone precursors, the SRF of nitrogen oxides (NO_x) is
28 the strongest, being for example about 16 times larger than and of opposite sign to CO SRF. It
29 is important to note that the strength of the SRF of a given NTCF is only one aspect of its
30 climate impact: the strength of anthropogenic emission rates is also important. Therefore, the
31 strong SRFs of BC and NO_x have to be considered in the context of their weak emission rates



1 relative to other NTCF precursors like sulphur dioxide (SO₂) and CO. SRF are however
2 useful to characterise the forcing characteristics of individual species in a context where the
3 amount of species emitted by a given economic sector varies in time because of changes in
4 technology or legislation (e.g. Smith et al., 2013).

5 The SRF estimates by Yu et al. (2013) are given for four regions (North America, Europe,
6 East Asia, South Asia), in contrast to the other studies listed in Table 1, which only take a
7 global view. They identified regional differences that appeared robust across participating
8 models. East Asian SO₂ emissions exert an SRF that is only 75% of that by European
9 emissions, a smaller value that Yu et al. (2013) attribute to a limitation in sulphur-cycle
10 oxidants over East Asia, which suppresses conversion of SO₂ to sulphate aerosols in that
11 region. Furthermore, their estimate of BC SRF from European emissions is 30% stronger than
12 that of other regions, a result attributed to the geographical extent of European aerosol
13 transport, which covers in particular the bright surfaces of the Arctic and Sahara, where BC
14 aerosols exert a strong positive RF.

15 Diversity in SRF estimates reflect diverse choices made when representing tropospheric
16 aerosols and chemistry in global models, uncertainties in understanding and representations of
17 radiative forcing mechanisms, and impacts of differences in other aspects of the host models.
18 Myhre et al. (2013b) found a sizeable range in aerosol optical properties among AeroCom
19 models. Also, different simulated vertical profiles affect RF efficiency, especially for
20 absorbing aerosols. For BC, Samset et al. (2013) suggest that different vertical distributions
21 explain 20% of RF diversity among AeroCom models. More generally for RFari interactions,
22 Stier et al. (2013) attribute a third of total AeroCom diversity to host model differences,
23 mainly coming from differences in cloud distributions, surface properties, and radiative
24 transfer, the latter contributing up to 20% (Randles et al., 2013). For RF of aerosol-cloud
25 interactions (RFaci), additional diversity comes from the parameterised sensitivity of cloud
26 albedo to aerosol changes, which varies by more than a factor 4 in AeroCom models (Quaas
27 et al., 2009). For ozone RF, Stevenson et al. (2013) estimate an overall uncertainty of 30% by
28 accounting for uncertainties in radiative transfer calculations (radiation schemes, simulated
29 clouds, and stratospheric adjustment techniques), diversity in simulated ozone levels in
30 present-day and pre-industrial conditions, uncertainties due to the identification of the



1 tropopause level, and uncertain climate change impacts on atmospheric dynamics and
2 chemistry.

3 Diversity is also introduced by the different treatment of modelled estimates in different
4 studies. For example, Myhre et al. (2013b) include all participating models in their estimates,
5 but Shindell et al. (2013) only select those models able to satisfactorily represent present-day
6 aerosol distributions and recent trends. Bond et al. (2013) scale modelled RF towards stronger
7 values mainly through increases in emissions to account for a perceived low bias in simulated
8 BC concentrations and absorption aerosol optical depth. This upward scaling has been
9 challenged by recent studies (Wang et al., 2014a; Samset et al., 2014), which argue that a
10 suite of observational constraints, including vertical profiles of BC concentrations in remote
11 regions, does not support the stronger end of the range in BC RF. Wang et al. (2014a) reduce
12 substantially the BC underestimation in their model compared to observations by improving
13 the model horizontal resolution. Samset et al. (2014) suggest that a majority of the aerosol
14 models overestimate BC lifetime, causing too strong an RF.

15 Conversely, multi-model inter-comparison studies do not generally consider all sources of
16 diversity in SRF estimates. Those studies typically mandate a common set of anthropogenic
17 emissions for all participating models, for example the emission dataset of Lamarque et al.
18 (2010) is used by AeroCom 2 and ACCMIP simulations. However, both present-day and pre-
19 industrial emissions are uncertain and that uncertainty, which can be substantial (Carslaw et
20 al., 2013), is not reflected in many of the ranges given in Table 1. Yu et al. (2013) include the
21 effect of different emission datasets being used by different models, but exclude another
22 source of diversity by using a single set of aerosol optical properties to derive their RF
23 estimates. The variable experimental designs of the studies listed in Table 1 hinder a clean
24 assessment of the metrics uncertainty caused by diversity in RF estimates (Fuglestedt et al.,
25 2010).

26 The Evaluating the CLimate and Air Quality ImPacts of Short-livEd Pollutants (ECLIPSE)
27 project (Stohl et al., 2015) covered in a consistent way the causal chain that links emissions of
28 NTCFs to their SRFs (this study), climate metrics (Aamaas et al., 2015) and the subsequent
29 climate response (Baker et al., 2015). This study documents the calculation of the ECLIPSE
30 matrix of SRF for NTCFs. Its aim is to provide a dataset of SRFs that spans the diversity



1 among models, while providing an explanation, albeit sometimes incomplete, for that
2 diversity.

3 SRFs are calculated for reductions in the anthropogenic emissions of primary aerosols (BC,
4 OC), aerosol precursors (sulphur dioxide, ammonia), ozone and secondary aerosol precursors
5 (NO_x, CO, VOC), and methane. This study shares common aspects with those listed in
6 Table 1, for example in the range of NTCFs considered. It is also a multi-model study, with
7 4 global circulation or chemistry-transport models participating. Like Yu et al. (2013), it takes
8 a regional view by focusing on two source regions, Europe and East Asia, and singling out the
9 shipping sector. But other aspects of this study are more distinctive. Emissions are perturbed
10 seasonally, to assess which of local summer or wintertime emission reductions are most
11 effective at exerting an SRF. This study also quantifies a larger number of radiative
12 mechanisms: RF_{aci} is systematically included, and ozone precursor RFs include a
13 contribution from aerosol changes that arise through aerosol-chemistry couplings.
14 Contributions to BC RF from deposition on snow and rapid adjustments from the semi-direct
15 effect are also estimated, albeit from a single model. Finally, although uncertainties in
16 emissions are not fully accounted for because all models participating in this study share the
17 same emission datasets, the large uncertainties in pre-industrial emissions are irrelevant here,
18 because the perturbations used in this study are defined as percentages of present-day
19 emissions.

20 The paper is structured as follows. Section 2 describes the participating models and
21 experimental design. Section 3 quantifies the components of SRF simulated by each model as
22 a function of emitted species, region, and season. Causes of model diversity are also identified
23 and discussed. Section 4 gives the best estimate of the SRF matrix resulting from the
24 ECLIPSE project. Finally, Sect. 5 concludes with a discussion of research priorities for
25 decreasing model diversity, and the challenges encountered when quantifying rapid
26 adjustments. Supplementary Figures show annually-averaged distributions of RF components
27 for all perturbations.

28



1 **2 Models and experimental protocol**

2 Participating models are ECHAM6-HAM2, HadGEM3-GLOMAP, NorESM1, and
3 OsloCTM2. It is known from previous participations of those models in multi-model inter-
4 comparisons, including the studies cited in the introduction, that the four models span a large
5 range of inter-model diversity for both aerosol and ozone. Horizontal and vertical resolution,
6 and the number of aerosol species included depend on the model (Table 2). In particular,
7 OsloCTM2 is the only model that represents nitrate aerosols. ECHAM6 does not simulate
8 secondary organic aerosols, and also lacks interactive ozone chemistry, and thus did not
9 perform perturbations to ozone precursor emissions.

10 ECHAM6-HAM2 is the European Centre for Medium-Range Weather Forecasts Hamburg
11 model version 6 (Stevens et al., 2013). Its radiation scheme is RRTM-G (Iacono et al., 2008).
12 Aerosols are represented by the two-moment Hamburg Aerosol Model (HAM) version 2
13 (Zhang et al., 2012), which consists of the microphysical module M7 that simulates seven
14 internally-mixed aerosol modes (Vignati et al., 2004; Stier et al., 2005). Aerosol interactions
15 with liquid and frozen water clouds follow Lohmann et al. (2007).

16 HadGEM3 is the Hadley Centre Global Environment Model version 3 (Hewitt et al., 2011).
17 Its radiation scheme is described by Edwards and Slingo (1996). Gas-phase chemistry is
18 modelled by the United Kingdom Chemistry and Aerosols (UKCA) TropIsop scheme, which
19 treats 55 chemical species (37 of which being transported) including hydrocarbons and
20 isoprene and its degradation products (O'Connor et al., 2014). Aerosols are coupled to the
21 chemistry, and modelled by UKCA-GLOMAP (GLobal Model of Aerosol Processes, Mann et
22 al., 2010), which represents the size-resolved internal mixture using a two-moment modal
23 approach and four soluble and insoluble aerosol modes. Aerosols interact with liquid clouds
24 only, following the empirical relationship between aerosol number and cloud droplet number
25 concentration established by Jones et al. (1994).

26 NorESM1-M is the Norwegian Earth System Model version 1 (Bentsen et al., 2013; Iversen et
27 al., 2013). Its atmosphere and aerosol module is CAM4-Oslo (Kirkevåg et al., 2013) and the
28 radiation scheme is described by Collins (2001). In the version used in this study, aerosols
29 (described by 20 tracers) are fully coupled to the MOZART tropospheric gas-phase chemistry
30 scheme (Emmons et al., 2010), which treats 84 gaseous species. Aerosol mass concentrations
31 are simulated in four size classes: nucleation, Aitken, accumulation, and coarse modes.



1 OsloCTM2 is the CTM of the University of Oslo and the Center for International Climate and
2 Environmental Research – Oslo (CICERO) (Myhre et al., 2009; Skeie et al., 2011). The
3 model is driven by meteorological data generated by the Integrated Forecast System (IFS)
4 model at the European Centre for Medium-Range Weather Forecasts (ECMWF). The model
5 simulates the tropospheric chemistry of 67 species (Dalsøren et al., 2007). Aerosols are
6 simulated as external mixtures of 7 aerosol types, including nitrate, as described by Skeie et
7 al. (2011). RFari and RFaci are computed by offline radiative transfer calculations, as
8 described in Myhre et al. (2007) and Skeie et al. (2011). Myhre et al. (2000) describes the
9 offline calculations performed to obtain ozone radiative forcing.

10 The 48 ECLIPSE RF simulations are listed in Table 3. Simulations are only 1-year long (after
11 spin-up) because RF by definition excludes changes in the tropospheric state and inter-annual
12 differences in meteorology are the only source of variability between simulations.
13 Meteorology affects transport and removal processes, especially wet deposition, and to a
14 lesser extent chemical production when driven by temperature or availability of sunlight.
15 Perturbation simulations made with HadGEM3 were extended to 3 years and suggest that
16 inter-annual variability never exceeds $\pm 10\%$ of globally-averaged RF, which is small
17 compared to inter-model diversity. RF is calculated at the top of the atmosphere as the
18 difference in net shortwave and longwave radiative fluxes between the perturbed and control
19 simulations.

20 Control emissions are taken from the ECLIPSE dataset version 4a (Stohl et al., 2015) for the
21 year 2008. A seasonal cycle has been applied to the emissions of the domestic sector, to
22 reflect changes in heating as a function of temperature. This seasonal cycle is obtained by
23 multiplying annual total domestic sector emissions by a gridded dataset of monthly weights,
24 obtained by the Mitigation of Arctic warming by Controlling European Black carbon
25 emissions (MACEB) project following Sect. 3.3 of Streets et al. (2003), where stove
26 operation times are expressed as a function of climatological monthly-mean temperature.

27 Emission perturbations involve a 20% decrease of primary and precursor emissions of the
28 given species in one of the following regions: Europe, East Asia, shipping, and Rest of the
29 World (RotW). Results for that last region are not presented directly in this paper: instead,
30 global results are given by adding Europe, East Asia, and RotW together. Applying a
31 decrease, rather than an increase, has been chosen because it better represents air quality and



1 climate policy objectives. The value of 20% was chosen to be representative of typical
2 technologically feasible emission reductions. The same value was also used in previous
3 HTAP simulations (Yu et al., 2013). The definition of regions also follows HTAP, more
4 specifically tier-1 HTAP regions. Regions are shown in Figure 2. Here, Europe includes
5 European Union and European Economic Area countries, and Switzerland, Turkey, and
6 former Yugoslavia. East Asia includes China, Japan, Taiwan, North and South Korea, and
7 Mongolia. Because of the specificity of the shipping sector in the policy agenda, its emissions
8 have been perturbed independently, with all species emitted by that sector being perturbed
9 together, although OsloCTM2 and NorESM1 have run perturbations for each species within
10 the shipping sector (results not shown). Shipping emissions are taken from the RCP6.0 dataset
11 (Fujino et al., 2006) prepared for phase 5 of the Climate Model Inter-comparison project
12 (CMIP5), interpolated to 2008 between 2005 and 2010. All perturbations are applied either in
13 Northern Hemisphere summer (May-October) or winter (November-April). The size of the
14 emission perturbations is given in Table 3, except for the shipping sector perturbations, which
15 are shown in Table 4. The size of shipping emission perturbations is different for ECHAM6-
16 HAM, because RCP8.5 (Riahi et al., 2007) was used, and for NO_x in NorESM1, because of a
17 mistake when processing that particular dataset. The size of non-methane VOC emission
18 perturbations is model-dependent because the list of species emitted under the VOC label
19 depends on the model used: 5 for HadGEM3, 14 for NorESM1, and 12 for OsloCTM2. For
20 OsloCTM2, VOC emissions were converted to unit mass of carbon by assuming a mean VOC
21 atomic weight of 47 u.

22 Methane perturbations are achieved by scaling the prescribed concentrations or mass-mixing
23 ratios, rather than by perturbing emissions like for the other NTCFs. This difference in
24 treatment arises because HadGEM3, NorESM1, and OsloCTM2 prescribe methane
25 concentrations at the surface and then let the chemistry scheme determine the vertical
26 distribution, thus avoiding long spin-ups caused by the 12-year lifetime of methane in the
27 atmosphere. Scaled methane surface concentrations C are given by the equation:

$$28 \quad C = C_0 \cdot (E/E_0)^f \quad (\text{Eq. 1})$$

29 where C_0 are the control surface concentrations, E is the global emission rate where the
30 anthropogenic contribution has been reduced by 20%, and E_0 is the control global emission
31 rate. E/E_0 is therefore equal to 0.8 in this study. f is the feedback factor of methane on its own



- 1 lifetime, defined as the ratio of methane perturbation lifetime to total budget lifetime. The
2 value of f for each participating model was not known when preparing the simulations, and
3 was therefore taken at 1.34 following Holmes *et al.* (2013). As discussed in Sect. 3.5, actual
4 values of f range from 1.28 to 1.46, in reasonable agreement with the value initially assumed.
5 Because the long atmospheric lifetime of methane allows it to be well mixed geographically,
6 methane perturbations are not applied regionally. NorESM1 applied perturbations seasonally
7 (May—Oct and Nov—Apr) and found differences in SRF of only 7% between the two
8 seasons. Because that seasonal dependence is small, OsloCTM2 and HadGEM3 have applied
9 the perturbation for the whole year.
- 10 Three methods are used to obtain stratospherically-adjusted RF from the perturbation
11 simulations, depending on the species being considered and whether the model is capable of
12 interactive radiation calculations (Table 1).
- 13 • To obtain the RF of aerosol perturbations in general circulation models, the model
14 evolution (“meteorology”) is set to be independent of the perturbation. The method used
15 to achieve this independence involves diagnosing radiative fluxes with and without the
16 forcing agent included, with the second set of radiative fluxes used to advance the model
17 into its next time step. Stratospheric adjustment is neglected for aerosols, because
18 tropospheric aerosol perturbations have little effect on stratospheric temperatures.
19 Aerosol RF includes both ari and aci, except for ECHAM6, which only diagnosed ari.
 - 20 • To obtain the RF of aerosol perturbations in chemistry-transport models and the RF of
21 ozone exerted by ozone-precursor perturbations in all models, instantaneous RF is
22 computed by offline radiative transfer codes, using aerosol and trace gas distributions
23 obtained from the perturbation simulations. HadGEM3 ozone RF is computed with the
24 offline version of the radiative transfer code by Edwards and Slingo (1996). OsloCTM2
25 aerosol and ozone RF, and NorESM1 ozone RF, are computed with offline longwave and
26 shortwave radiative transfer codes as described earlier in this section. For all models,
27 ozone RF is adjusted for changes in stratospheric temperatures.
 - 28 • The RF of methane is computed using the analytical expression established by Myhre *et*
29 *al.* (1998), which accounts for stratospheric adjustments. Details of this calculation are
30 given in Sect. 3.5 below.



1 The four models simulate different aerosol and tropospheric ozone lifetimes, as shown in
2 Table 5. Sulphate aerosol lifetime varies by a factor 1.5, from 3.5 to 5.2 days. All models
3 agree that BC lifetime is longer, with a diversity similar to sulphate, with variations by a
4 factor 1.5, from 5.2 to 8.0 days. Modelled OC lifetime is also longer than that of sulphate,
5 with a large diversity, with variations by a factor 2.5, from 3.1 to 7.7 days. Tropospheric
6 ozone lifetime is also diverse: HadGEM3 and NorESM1 disagree by a factor 1.3, from 20.7 to
7 26.4 days. OsloCTM2 did not diagnose it. Differences in simulated lifetimes are thought to
8 arise from virtually all aspects of the models, including differences in the simulated present-
9 day climate, the treatment of atmospheric horizontal and vertical transport, atmospheric
10 chemistry, and wet and dry deposition processes. Large model spreads have long been a
11 characteristics of aerosol and chemistry inter-comparisons (e.g. Myhre et al., 2013b;
12 Stevenson et al., 2013), in part because of a lack of strong observational constraints on
13 atmospheric lifetimes on a global scale (Kristiansen et al., 2012; Hodnebrog et al., 2014). The
14 four ECLIPSE models are representative of those spreads, which will affect the range of SRF
15 they simulate.

16

17 **2.1 Biases and scaling of specific radiative forcing**

18 Aerosol and ozone distributions simulated by the four models participating in this study have
19 been compared to observations as part of their development cycles, multi-model inter-
20 comparisons, and within the ECLIPSE project. Those evaluations draw a complex picture,
21 where model skill at reproducing NTCF distributions with fidelity differs among models and
22 is strongly region- and species-dependent.

23 To ensure the relevance of evaluations to the SRF matrix, they are discussed for each species
24 alongside SRF results in Sect. 3. This section focuses on the evaluation of two cross-cutting
25 quantities: aerosol optical depth (AOD) and ozone concentrations. To reproduce the
26 magnitude and geographical distribution of those two quantities accurately, one needs to
27 simulate several aerosol species and ozone precursors well.

28 ECLIPSE evaluation of AOD focused on East Asia. Patterns of total AOD simulated by the
29 four models over East Asia compare well against MODIS (Moderate Resolution Imaging
30 Spectroradiometer) aerosol retrievals, but fail quantitatively to various extents depending on



1 model, season, and region (Quennehen et al., 2015). NorESM1 and, to a larger extent,
2 HadGEM3 overestimate the AOD background. HadGEM3 also overestimates AODs over
3 East Asia, while they are underestimated by ECHAM6 and OsloCTM2. Models are similarly
4 diverse in their ability to reproduce the temporal variability of AOD: NorESM1 ranks best in
5 Eastern China, but HadGEM3 and OsloCTM2 do better in northern India. In the vertical,
6 comparing the four models to the vertical profiles of aerosol scattering retrieved by the Cloud-
7 Aerosol Lidar with Orthogonal Polarization (CALIOP) shows that models underestimate
8 aerosol scattering in the lowest 2 km of the atmosphere, but overestimate it at altitudes
9 ranging from 2 to 4 km, hinting at too efficient a transport into the free troposphere or too
10 weak sinks (Quennehen et al., 2015). For RFaci, such errors in simulated vertical profiles may
11 lead to too weak an SRF, because aerosols that should have interacted with clouds end up
12 being simulated above those clouds, unable to interact with them. For BC, placing the
13 aerosols too high in the atmosphere leads to overestimating RFari (Samset et al., 2013) but
14 underestimating rapid adjustments from semi-direct effects, so the net impact on SRF depends
15 on the local balance between those two mechanisms.

16 For tropospheric ozone, Schulz et al. (2015) evaluated the surface concentrations of ozone
17 simulated by OsloCTM2 and NorESM1 models over Europe. They find that OsloCTM2
18 reproduces magnitude and seasonality very well, but that NorESM1 has a high bias,
19 especially in Northern Hemisphere winter. HadGEM3 could not be part of that evaluation, but
20 an evaluation of an earlier version of the model indicates that it captures well the seasonality
21 and magnitude of ozone surface concentrations at mid-latitude of the NH, but has a high bias
22 in the Tropics and high latitudes (O'Connor et al., 2014). Over Asia, Quennehen et al. (2015)
23 find that HadGEM3, NorESM1 and OsloCTM2 simulate total column ozone within 10%,
24 with OsloCTM2 having essentially no bias against infrared sounder observations and
25 HadGEM and NorESM1 both overestimating the ozone column. The three models locate
26 ozone too low in the troposphere, as evidenced by an increase in positive biases by 3 to 7% in
27 the 0–6 km layer. The models are able to qualitatively reproduce the gradients existing
28 between surface concentrations in urban and rural conditions, but modelled gradients are
29 smoothed out because of the relatively coarse resolutions of the models.

30 RF and SRF cannot be evaluated against observations, so the challenge is to interpret what
31 regional evaluations of surface concentrations, vertical profiles and optical properties imply



1 for globally-averaged SRF to regional perturbations. As a general guideline, biases in mass
2 concentrations or optical depth should not be expected to propagate fully into biases in SRF,
3 because of its normalisation to emission rates. Biases would not propagate in regions where
4 concentrations and AOD scale linearly with emissions, for example where oxidants do not
5 limit sulphate or ozone formation, and where RF scales linearly with concentrations and
6 AOD, as is for example mostly the case for aerosol-radiation interactions. However, biases in
7 lifetime and local concentrations become important on a global scale when a model fails to
8 transport an NTCF to a region where RF efficiency is significantly different to its source
9 region, for example where surfaces are highly reflective (deserts, ice, and snow) or the cloud
10 regime is strongly susceptible to aerosol influences (low maritime clouds).

11 In addition, there are known non-linearities in the emission-concentration-RF chain. Methane
12 RF is proportional to the square root of its concentration (Myhre et al., 1998). Aerosol-cloud
13 interactions are non-linear because strong non-linearities between aerosol and CCN
14 concentrations (Hegg, 1994) combine with strong non-linearities between cloud droplet
15 concentrations and cloud albedo (Taylor and McHaffie, 1994). Aerosol-cloud interactions will
16 therefore desaturate more quickly in regions where aerosol concentrations are small to
17 moderate: this is where biases in concentrations will have strong impacts on RF estimates.
18 Conversely, errors in simulating the large concentrations in polluted regions will have a lesser
19 impact. In contrast, errors in simulating vertical profiles can have disproportionate impacts
20 on SRF for species that absorb in the shortwave spectrum. Locating BC aerosols too high up
21 in the atmosphere will systematically overestimate their RF because aerosol absorption is
22 enhanced when overlying bright surfaces such as clouds. Hodnebrog et al. (2014) show that
23 reducing lifetime by 40% to 3.9 days to improve the match to observed BC vertical profiles
24 reduces the forcing approximately by a factor of two. Ozone adjusted RF is similarly altitude-
25 dependent because of varying degrees of compensation between the shortwave and longwave
26 components of RF. In the troposphere, where this study's ozone perturbations are located,
27 ozone RF efficiency increases with altitude with a maximum near the tropopause (Lacis et al.,
28 1990). The fact that the models locate ozone too low in the atmosphere would therefore
29 introduce a low bias in the SRF exerted by ozone precursors.

30 To summarise, regional and seasonal variations in model skill at simulating aerosols and
31 ozone with fidelity, the normalised nature of SRF, and non-linearities in the emission-to-



1 forcing chain preclude a simple scaling of modelled SRF with identified biases. So this study
2 reports SRF as simulated by the models, discussing where appropriate in the next section the
3 implications of comparisons to observations for the SRF exerted by each species.

4

5 **3 Specific radiative forcing by species**

6 In this section, SRFs of each primary or precursor species are discussed in turn. SRF is
7 stratospherically-adjusted but excludes rapid adjustments in the troposphere, with one
8 exception: rapid adjustments of BC semi-direct effects have been computed independently
9 and are discussed in Sect. 3.2. SRF is given for May-October (hereafter labelled Summer for
10 the sake of simplicity but also because emission perturbations are disproportionality located in
11 the Northern hemisphere) and November-April (labelled Winter), for three regions (Europe,
12 East Asia, and Global), and for the shipping sector. Globally-averaged RF is computed as the
13 sum of the European, East Asian, and RotW perturbations. Although perturbations are not
14 exactly additive, this is a good first-order assumption.

15 **3.1 Sulphur dioxide**

16 Figure 3 shows globally- and annually-averaged SRF for sulphur dioxide perturbations in the
17 four ECLIPSE models. SO₂ SRF ranges from $-1.2 \text{ mW m}^{-2} (\text{Tg}[\text{SO}_2] \text{ yr}^{-1})^{-1}$ for the European
18 Winter perturbation by ECHAM6 to $-18.0 \text{ mW m}^{-2} (\text{Tg}[\text{SO}_2] \text{ yr}^{-1})^{-1}$ for the European Summer
19 perturbation by HadGEM3. ECHAM6 is consistently associated with weak SRF because it
20 only diagnoses ari. On a global scale, ari account for 43% and 55% of total RF according to
21 NorESM1 and OsloCTM2, respectively, which diagnosed ari and aci separately. The ari
22 contribution varies seasonally, being generally stronger in Winter than in Summer
23 perturbations in both models. They also vary regionally, but in a model-dependent way:
24 OsloCTM2 obtains the largest contribution of ari in Europe, but NorESM1 locates it in East
25 Asia. Note that only ari and aci RF mechanisms are considered here: ozone and methane RF
26 exerted by perturbations to OH distributions resulting from perturbations of SO₂ emissions are
27 negligible.

28 All models agree that SO₂ SRF is stronger for Summer than Winter perturbations, which is
29 expected because sulphate RF_{ari} and RF_{aci} act almost exclusively in the shortwave spectrum



1 and are therefore a strong function of solar irradiance. As shown in Figure S1, sulphate RF
2 covers a larger area in models with longer sulphate aerosol lifetimes, such as HadGEM3, than
3 in models with shorter lifetimes, like OsloCTM2. This extended coverage has two competing
4 effects on the strength of SRF, both driven by non-linearities in RFaci. On the one hand, a
5 longer lifetime promotes stronger RFaci because emission perturbations propagate more
6 easily to remote regions where concentrations are low and RFaci desaturates more easily. On
7 the other hand, a longer lifetime weakens RFaci by increasing concentrations in the reference
8 simulation in those same remote regions, saturating RFaci. The first effect dominates in the
9 ECLIPSE models because SRF strength increases with lifetime. RFaci non-linearities also
10 explain why models simulate weaker SRFs for East Asian than European perturbations. With
11 a more polluted baseline, East Asian aci stands more often at the saturated end of the CCN-
12 cloud albedo relationship, where RFaci is weak (Wilcox et al., 2015).

13 Non-lifetime related aspects will also increase diversity in SO₂ SRF. Firstly, the
14 parameterised strength of aci varies between models (Quaas et al., 2009). Secondly, models
15 have different cloud climatologies (Jiang et al., 2012): aerosols being more likely to be co-
16 located with low clouds, low cloud amounts influence RFaci. Thirdly, the relatively weak SO₂
17 SRFs simulated by OsloCTM2 are partly due to the inclusion of nitrate aerosols in that model.
18 Ammonium nitrate formation is suppressed by that of ammonium sulphate, meaning that a
19 reduction in SO₂ emissions indirectly favours nitrate formation (Bellouin et al., 2011). The
20 RF exerted by the increase in nitrate aerosol weakens the overall SRF. In OsloCTM2, nitrate
21 RFari offsets 4 to 10% of sulphate RFari, with larger offsets obtained in Northern Hemisphere
22 winter months.

23 In Europe, ECLIPSE models underestimate sulphate aerosol surface concentrations, in part
24 because of underestimated SO₂ oxidation rates (Schulz et al., 2015). In the Arctic, Eckhardt et
25 al. (2015) report that models underestimate winter/spring sulphate concentrations by an
26 average factor of 2, with longer-lived aerosols yielding no improvement against observations,
27 suggesting that transport of aerosols to the Arctic is only part of the problem. Although those
28 concentration biases may not affect SRF, the fact that models fail to reproduce the observed
29 summer minimum in the Arctic, as reported by Eckhardt et al. (2015), suggests that SRF may
30 be too weak in magnitude in that region.



1 Changes in sulphate aerosols may exert rapid adjustments that follow the perturbation to
2 cloud droplet size distributions. Those are not quantified here, because ECLIPSE models do
3 not yet adequately represent the observed dependence of the strength and sign of rapid
4 adjustments on cloud regime (Christensen and Stephens, 2011). In addition, rapid adjustments
5 are difficult to isolate robustly from internal variability in top-of-atmosphere radiative fluxes,
6 especially for the small perturbations imposed in this study.

7

8 **3.2 Black carbon aerosol**

9 Figure 4 shows globally- and annually-averaged SRF for BC aerosol perturbations in the four
10 ECLIPSE models. BC SRF ranges from $+3.7 \text{ mW m}^{-2} (\text{Tg}[\text{C}] \text{ yr}^{-1})^{-1}$ for the East Asian Winter
11 perturbation by HadGEM3 to $+139.8 \text{ mW m}^{-2} (\text{Tg}[\text{C}] \text{ yr}^{-1})^{-1}$ for the Global Summer
12 perturbation by the same model. BC SRF is positive because ari and snow-albedo
13 mechanisms both exert positive RFs due to the strong absorption of shortwave radiation
14 associated with BC aerosols. However, negative RF from aci and rapid adjustments from the
15 semi-direct effect partly offset those positive contributions. Note that changes in primary BC
16 emissions are also associated with ozone and methane RF because of changes in the surface
17 of aerosols available for heterogeneous reactions, but the resulting RFs are negligible and not
18 reported in this study. The relatively weak BC SRF by ECHAM6 is partly due to the lack of
19 diagnosis of RFaci, although ari strongly dominate, with RFaci representing only 2 to 15% of
20 its RFari according to NorESM1 and OsloCTM2.

21 BC SRF is stronger for Summer than Winter perturbations in all models, which is expected
22 for RF mechanisms that act primarily on shortwave radiation. BC SRF is not clearly
23 correlated to modelled lifetimes, contrary to what is found for sulphate. The lack of
24 correlation has three main causes. First, the strength of BC RFari is strongly modulated by the
25 albedo of the underlying surface: for a given optical depth and single-scattering albedo, BC
26 aerosols exert a stronger RFari when located above bright surfaces, like deserts, snow and ice,
27 and clouds. So BC transport to remote regions by longer lifetimes affects the diversity of
28 surface albedos experienced by the BC aerosols in a complex way. Figure S2 shows for
29 example that the long lifetime of BC in NorESM1 translates into a strong RF over the Arctic
30 for East Asian and Global perturbations. Other models have weaker RFs because the same



1 perturbations affect the Arctic in a weaker way. NorESM1's BC lifetime may however be too
2 long, because it overestimates BC concentrations in the Arctic (Eckhardt et al., 2015).
3 Secondly, BC mass-absorption coefficients (MAC) vary among models because those models
4 make different prescriptions of refractive indices and different assumptions of mixing state
5 and hygroscopic growth. Globally-averaged BC MAC for ambient conditions is $10.4 \text{ m}^2 \text{ g}^{-1}$ in
6 ECHAM6, $15.7 \text{ m}^2 \text{ g}^{-1}$ in HadGEM3, only $3.8 \text{ m}^2 \text{ g}^{-1}$ in NorESM1, and varies between
7 $7.3 \text{ m}^2 \text{ g}^{-1}$ for hydrophobic and $11.0 \text{ m}^2 \text{ g}^{-1}$ for hydrophilic BC in OsloCTM2. Finally, the
8 impact of the aerosol mixture can be complex. For example, HadGEM3 simulates negative
9 BC SRFs over northern Russia for the Global Summer perturbation (Figure S2). The reason is
10 that perturbations of primary BC emissions also perturb condensation of organic materials in
11 that model: by having fewer primary particles, the gaseous condensation sink is suppressed,
12 favouring the nucleation of new CCNs in pristine regions (Bellouin et al., 2013).

13 ECLIPSE models generally underestimate BC aerosol surface concentrations in Europe
14 (Schulz et al., 2015). In the Arctic, Eckhardt et al. (2015) find underestimates by factors 4 to
15 27 in the four models, especially HadGEM3, in all seasons, except for NorESM1 which
16 overestimates concentrations by a factor 1.3 in summer. Those incorrect estimates occur
17 throughout the troposphere, although aircraft campaigns are biased high by targeting
18 biomass-burning aerosol plumes rather than average background conditions. Eckhardt et al.
19 (2015) conjecture that emissions are underestimated, especially in northern Russia. Modelled
20 BC has not been evaluated in India, but Gadhavi et al. (2015) also find that the BC emission
21 rates used in ECLIPSE are likely underestimated. BC being a primary aerosol, it is therefore
22 probable that Indian concentrations are underestimated as well. Those biases would not bias
23 the SRF unless radiative efficiency is also biased, and there are indications that models
24 systematically overestimate BC concentrations in the remote troposphere, especially at higher
25 altitudes (Samset et al., 2014). The SRF would therefore be too strong. Hodnebrog et al.
26 (2014) confirm this assessment and argue that BC emissions are underestimated in models
27 while lifetimes are too long. They find that those overestimated lifetimes lead to an
28 overestimate of BC SRF by a factor of around 2.

29 Absorbing AODs offer an indirect constraint on BC concentrations, at least in regions where
30 mineral dust aerosols are not present and assuming that OC aerosols do not strongly
31 contribute to absorption, which may not be true in biomass-burning regions (Saleh et al.,



1 2014). Compared to AERONET retrievals, the four ECLIPSE models underestimate
2 absorbing AOD by more than a factor 2 (Schulz et al., 2015). The constraint brought by
3 AERONET absorption retrievals is however debated because its retrieval algorithm requires
4 large solar zenith angles and has large uncertainties at low AODs (Dubovik et al., 2000).
5 AERONET absorbing AODs are therefore only reported for morning/evening conditions and
6 for thicker plumes, which may introduce systematic biases by not sampling background
7 aerosols. In addition, Wang et al. (2015) showed that the fairly low resolutions of global
8 models similar to those used in this study induce an artificial negative bias when comparing to
9 AERONET stations in Asia.

10 The RF due to BC deposition on snow, shown in grey in Figure 4, is only quantified by
11 OsloCTM2. It is a small term globally, and negligible for Summer perturbations because
12 fossil-fuel BC sources are mostly located in the Northern Hemisphere where snow cover is
13 minimum during May to October. Winter perturbations exert stronger BC-on-snow RFs,
14 which represent 15, 20, and 53% of RF_{air} for Global, East Asian, and European perturbations,
15 respectively. The disproportionately strong contribution of the European perturbation is due to
16 its geographical location: in spite of smaller BC emitted mass in Europe, Arctic RF is similar
17 to that of East Asian emission perturbations (Figure S3). The BC-on-snow SRF exerted by the
18 European Winter perturbation is, at $17 \text{ mW m}^{-2} (\text{Tg}[\text{C}] \text{ yr}^{-1})^{-1}$, 3.4 times stronger than for the
19 East Asian Winter perturbation and 2.4 times stronger than for the Global Winter
20 perturbation, also because of Europe's proximity to the Arctic. Jiao et al. (2014) assessed an
21 offline land surface model with BC deposition rates simulated by AeroCom models, including
22 OsloCTM2. They find that OsloCTM2 is among the models that overestimate BC-in-snow
23 amounts the most compared to measurements in the Arctic, suggesting a possible
24 overestimation of BC-on-snow SRF in this study.

25 BC aerosols are unusual among NTCFs because their strong absorption of shortwave
26 radiation is expected to trigger strong rapid adjustments (Koch and Del Genio, 2010), which
27 have been observed in marine stratocumulus regimes (Brioude et al., 2009; Wilcox, 2010).
28 Quantifying those rapid adjustments on a global scale is a challenge, because they are small
29 compared to internal variability in cloud fraction and top-of-atmosphere radiative fluxes.
30 Here, the quantification is done by prescribing control and perturbed distributions of BC
31 mass-mixing ratios simulated by OsloCTM2 into the Community Earth System Model



1 (CESM) version 1.0.4 (Neale et al., 2010). 30-year CESM simulations use fixed sea-surface
2 temperatures in order to suppress the long-term climate response and isolate the ERF. RFari
3 was quantified using multiple calls to the radiation scheme, following Ghan (2013). Because
4 aci are not included in the CAM4 atmospheric component of the CESM, the rapid
5 adjustments from the semi-direct effects of BC are calculated by subtracting its RFari from
6 total ERF. The reference CESM simulation uses BC concentrations taken directly from the
7 reference OsloCTM2 simulation. Then, to improve the signal-to-noise ratio between ERF and
8 unforced variability in perturbation simulations, the changes in BC are scaled before being
9 prescribed in CESM, following the equation:

$$10 \quad BC_{\text{CESM}} = (BC_{\text{REF}} - BC_{\text{PERT}}) * S + BC_{\text{REF}} \quad (\text{Eq. 2})$$

11 where BC_{CESM} are the distributions of BC concentrations prescribed into CESM, BC_{REF} and
12 BC_{PERT} are OsloCTM2's reference and perturbed distributions, respectively, and S is a scaling
13 factor. Table 6 gives the scaling factors imposed. The smaller the perturbation, the larger the
14 scaling factor required. Therefore, European perturbations are scaled by a factor 500 but
15 RotW perturbations only require a scaling factor of 30. The application of such large scaling
16 factors requires that rapid adjustments from the semi-direct effect scale linearly with the BC
17 perturbation imposed. This has been checked by imposing increasing scaling factors of 15, 50,
18 150, and 1500 to the East Asian Summer perturbation. Corresponding semi-direct SRFs are
19 -44 ± 121 , -38 ± 40 , -38 ± 12 , and $-35 \pm 1 \text{ mW m}^{-2} (\text{Tg}[\text{BC}] \text{ yr}^{-1})^{-1}$, indicating a
20 satisfactory level of linearity and supporting the application of large scaling factors.

21 Table 6 also gives the statistics of the resulting semi-direct SRFs taken over the 30 years of
22 simulation. With the exception of the East Asian Winter perturbation, semi-direct SRF is
23 negative, thus opposing the positive BC RFari. Semi-direct SRFs are weaker in Winter than in
24 Summer perturbations, as expected from a mechanism driven by absorption of shortwave
25 radiation. There are no strong regional variations in semi-direct SRFs. In spite of the large
26 scaling factors imposed, statistics are fragile and 90%-confidence intervals include 0 mW m^{-2}
27 for Winter perturbations. It is therefore important to keep in mind that the semi-direct
28 component of BC SRF is even more uncertain than the other components, and may not be
29 significantly different from zero.

30



1 3.3 Organic carbon aerosol

2 Figure 5 shows globally- and annually-averaged SRF for perturbations to primary organic
3 carbon aerosol emissions in the four ECLIPSE models. OC SRF ranges from +1.2 mW m⁻²
4 (Tg[C] yr⁻¹)⁻¹ for the East Asian Winter perturbation by ECHAM6 to -32.5 mW m⁻² (Tg[C]
5 yr⁻¹)⁻¹ for the European Summer perturbation by NorESM1. ECHAM6 is again consistently
6 associated with weak SRF because it only diagnoses ari. NorESM1 and OsloCTM2 disagree
7 on the fraction of total RF contributed by ari. In OsloCTM2, ari dominates by contributing
8 77-83% of total SRF for European and East Asian perturbations and 63-67% for the Global
9 perturbation. Winter perturbations are associated with slightly larger contributions of ari. In
10 contrast, NorESM1 simulates a domination of aci, with ari only contributing 11-31% of total
11 SRF for European and East Asian perturbations and 22-23% for the Global perturbation.
12 Differences between seasons and regions are also more pronounced than in OsloCTM2. As
13 for BC aerosols, changes in primary OC emissions are also associated with ozone and
14 methane RF because of changes in the surface of aerosols available for heterogeneous
15 reactions, but the resulting RFs are negligible and not reported in this study.

16 OC RF extends to larger areas (Figure S4) for models with longer lifetimes (Table 5),
17 although the correlation between lifetime and SRF is not as clear as for SO₂ perturbation
18 simulations. All models agree that OC SRF is stronger for Summer than Winter perturbations,
19 which is expected for shortwave aerosol radiative effects. In addition, the four models suggest
20 that European perturbations exert stronger SRFs than East Asian perturbations, which can be
21 expected from a less polluted baseline in Europe.

22 OC aerosol surface concentrations are generally underestimated in Europe (Schulz et al.,
23 2015) and at urban, remote, and marine sites worldwide (Tsigaridis et al., 2014). Those
24 underestimations are attributed to underestimated sources in models, including primary
25 emissions and secondary aerosol formation. Those underestimations may however not bias
26 the SRF published in this study for the reasons discussed in Sect. 2.1.

27 Like sulphate aerosols, OC aerosols may exert rapid adjustments through changes in cloud
28 microphysics. However, confidence in the ability of global models to represent those
29 mechanisms with fidelity is low (Stevens and Feingold, 2009), so those adjustments are not
30 quantified here.



1

2 **3.4 Ammonia**

3 Ammonia (NH_3) is, with nitrogen oxides, the precursor to ammonium nitrate aerosol.
4 Ammonia perturbations have only been simulated by OsloCTM2 because it is the only
5 participating model that represents the equilibrium between nitric acid, which is in the gas
6 phase, and nitrate aerosols. Globally- and annually-averaged SRF for ammonia perturbations
7 are shown in Figure 6. OsloCTM2 attributes 72 to 93% of SRF to ari, with larger fractions for
8 Winter perturbations. In spite of nitrate aerosols having similar optical and cloud nucleus
9 properties as sulphate aerosols, their simulated SRFs are about 10 times weaker at -1 mW m^{-2}
10 $(\text{Tg}[\text{NH}_3] \text{ yr}^{-1})^{-1}$. This weakness is due to two factors. First, formation of ammonium nitrate
11 competes against that of ammonium sulphate, which is favoured by its better
12 thermodynamical stability (Metzger *et al.*, 2002). The efficiency of nitrate precursor
13 reductions therefore depends on regional sulphur dioxide levels. Second, nitrate aerosols are
14 semi-volatile and dissociate back into the gas phase when temperatures increase. Nitrate
15 aerosol formation is therefore hindered during daytime (Dall'Osto *et al.*, 2009), decreasing
16 the ability of nitrate aerosols to interact with radiation. Sulphate aerosols have a more stable
17 diurnal cycle, maximising their radiative forcing efficiency. Figure S5 shows distributions of
18 nitrate RF simulated by OsloCTM2, which remains located near the perturbed regions,
19 suggesting a short lifetime. That lifetime has however not been quantified in the model.

20 In AeroCom simulations of industrial-era RFari, 8 models with nitrate representations
21 produced estimates of nitrate RF efficiency that range from 60 to 160% of the 8-model
22 median of $-155 \text{ W g}[\text{NO}_3]^{-1}$ (Myhre *et al.*, 2013b). Diversity in SRF will be at least as large,
23 with diversities in lifetimes and aerosol-cloud interactions also contributing. Modelled nitrate
24 lifetimes reported for present-day conditions in the literature indicate that this source of
25 diversity is likely to be sizeable, with Bellouin *et al.* (2011) obtaining 3.1 days and
26 Hauglustaine *et al.* (2014) having 4.6 days (50% longer). Diversity to aerosol-cloud
27 interactions is most probably similar to the 10% reported for sulphate aerosols in Sect. 3.1.
28 Overall, a conservative estimate of diversity is a factor of 2 each side of the OsloCTM2
29 estimate of nitrate SRF given here.

30



1 **3.5 Methane**

2 As discussed in Sect. 2, methane perturbations have been applied globally and annually,
3 instead of regionally and seasonally. This simplification is motivated by technical
4 considerations, because the long lifetime of methane would necessitate long model spin-ups.
5 However, this long lifetime also means that methane is relatively well mixed in the
6 atmosphere compared to shorter-lived species, thus the regional and seasonal nature of
7 perturbations are quickly lost, all perturbations converging into similar SRFs. This
8 convergence has been checked in NorESM1, where Summer and Winter perturbations have
9 been applied and found to yield methane SRFs that differ by only 7%.

10 The SRF exerted by methane itself is computed analytically on a global average in a four-
11 stage calculation.

12 - First, the methane feedback factor f is derived from each model using Eq. 2 and 3 of
13 Stevenson *et al.* (2013), which require the knowledge of control and perturbed methane
14 burdens, and total methane lifetime τ_{tot} . Following Stevenson *et al.* (2013), τ_{tot} accounts for
15 three methane sinks: destruction by OH, which is diagnosed in each model; losses to the
16 stratosphere, with a lifetime taken at 120 years; and losses to the soils, with a lifetime taken at
17 160 years. Those two lifetimes are also taken from Stevenson *et al.* (2013). ECLIPSE
18 feedback factors range from 1.28 to 1.46 (Table 7), in close agreement with the multi-model
19 mean derived by Holmes *et al.* (2013).

20 - In a second step, the equivalent methane emission perturbation ΔE is computed as

$$21 \quad \Delta E = \Delta B / (f * \tau_{\text{tot}}) \quad (\text{Eq. 3})$$

22 where ΔB is the change in burden between the control and perturbed simulations.

23 - The third step computes methane RF in each model by inserting control and perturbed
24 methane volume mass-mixing ratios in the formula established by Myhre *et al.* (1998). The
25 mass-mixing ratio of nitrous oxide (N₂O), which is required to apply the formula, is taken at
26 325 ppb (WMO, 2014).

27 - Finally, methane SRF is computed as the RF divided by ΔE , and increased by 15% to
28 represent the increase in stratospheric water vapour that follows methane oxidation (Myhre *et*
29 *al.*, 2007b).



1 Methane burdens, lifetimes, and all the global averages involved in computing the methane
2 contribution to total methane SRF in the three ECLIPSE models, are given in Table 7. It is
3 important to note that the diversity in modelled methane SRF is not due to uncertainties in the
4 radiative properties of the molecule, but rather due to the diversity in simulating present-day
5 burdens, which affect the baseline of a non-linear RF.

6 In addition to the SRF exerted by methane itself, components due to perturbations to aerosols
7 and ozone precursors contribute to total methane SRF (Figure 7). Aerosol and ozone RFs are
8 derived using the methods described in Sect. 2.

9 The aerosol component of methane SRF arises from the increase in OH that follows the
10 decrease in CH₄ concentrations. This increase promotes SO₂ oxidation into sulphate aerosols,
11 contributing a negative RF that, once divided by the negative methane emission change,
12 translates into a positive contribution to total SRF. That contribution is very diverse among
13 models, varying from a weakly negative contribution in OsloCTM2 to a strongly positive
14 contribution in HadGEM3. The OsloCTM2 value is from a simplified calculation, using
15 distributions of radiative forcing efficiencies instead of the full radiative transfer calculations
16 used by the other models and for the other perturbations. This simplified calculation only
17 represents ari, and the OsloCTM2 aerosol contribution would likely be positive, like the other
18 models, if aci were included. But three other aspects of the models contribute to the diversity
19 in estimates of aerosol contributions to methane SRF. The first aspect is the size of the
20 relative increase in global OH burden that follows the decrease in methane concentrations
21 imposed in ECLIPSE. NorESM1 and OsloCTM2 obtain similar global averages, at +4.5%
22 and +4.6%, respectively, but HadGEM3 simulates a larger sensitivity of OH, at +7%.
23 Secondly, other limitations restrict the aerosol response in some models, but not others. For
24 example, NorESM simulates aerosol SRFs of differing signs (Figure S6), which indicate
25 different responses of local chemistry, possibly mediated by changes in oxidation pathways
26 by O₃ and H₂O₂. In HadGEM3 however, aerosol SRF is uniformly positive across the globe
27 (Figure S6), indicating that once OH is increased, no further limitation restricts the size of the
28 aerosol response. The realism of those responses are difficult to confirm from observations, as
29 evidence for changes in the oxidising capacity of the atmosphere are lacking. Thirdly, the
30 inclusion of nitrate aerosols in OsloCTM2 counteracts the sulphate aerosol response, because



1 increases in ammonium sulphate aerosol formation are detrimental to ammonium nitrate
2 aerosol formation.

3 In stark contrast to the diversity seen in the aerosol component of total methane SRF, all three
4 models simulate ozone contributions to methane SRF close to one third of the SRF of
5 methane itself. This chemical feedback is therefore in good agreement among models, and is
6 proportional to the size of the methane perturbation. Figure S7 shows that the models also
7 agree well on the geographical distribution of the ozone SRF, with a maximum at the tropical
8 boundaries.

9

10 **3.6 Nitrogen oxides**

11 Figure 8 shows globally- and annually-averaged SRF for nitrogen oxide perturbations in the
12 three ECLIPSE models with tropospheric ozone chemistry schemes. Total NO_x SRF varies
13 from $-0.16 \text{ mW m}^{-2} (\text{Tg}[\text{NO}_2] \text{ yr}^{-1})^{-1}$ for the East Asian Summer perturbation with
14 NorESM1 to $-1.97 \text{ mW m}^{-2} (\text{Tg}[\text{NO}_2] \text{ yr}^{-1})^{-1}$ for the Global Winter perturbation with
15 OsloCTM2. SRF components are region- and season-dependent, but the dependence of net
16 SRF is less pronounced because the short-lived ozone and aerosol contributions compensate
17 each other. Total NO_x SRF is negative in all models for all regions and seasons, but results
18 from the addition of negative contributions by methane and primary-mode ozone SRF and
19 positive contributions by short-lived changes in ozone. Models disagree on the sign of the
20 aerosol contribution. Quantitatively, the three models are in good agreement on the SRF
21 exerted directly by ozone, both on a global average (Figure 8) and on patterns (Figure S9) but
22 disagree on the contributions of methane/primary-mode ozone and aerosols.

23 The methane and primary-mode ozone SRF are calculated as global averages only, by
24 multiplying the change in methane burden due to its reaction with OH by a radiative forcing
25 efficiency (RFE). Methane RFE is taken at $0.363 \text{ mWm}^{-2} \text{ ppbv}^{-1}$ (Table 8.A.1 of Myhre et al.,
26 2013a). Primary-mode ozone RFE is computed as the ratio of ozone RF to total methane
27 burden change in the methane perturbation simulations (see Sect. 3.5). That RFE is more
28 easily expressed as a fraction of the methane RFE, with good agreement among ECLIPSE
29 models: 0.396 for HadGEM3, 0.385 for NorESM1, and 0.395 for OsloCTM2. Figure 8 shows
30 that the resulting methane and primary-mode ozone SRF are in good agreement between



1 OsloCTM2 and NorESM1 for NO_x perturbations, but HadGEM3 simulates a weaker SRF.
2 This is consistent with results from the methane perturbation (Table 7).
3 Models strongly disagree on the aerosol contribution to NO_x SRF. That contribution is
4 generally negative, but NorESM1 also simulates positive contributions, especially in Winter
5 perturbations. In an absolute sense, the strongest contributions are simulated by OsloCTM2
6 for Europe and East Asian Summer perturbations, and by HadGEM3 for East Asian Winter
7 and Global perturbations. Figure S8 shows that those disagreements stem from differences in
8 regional responses. Both HadGEM3 and NorESM1 show positive aerosol RFs centred on the
9 regions being perturbed, caused by a decrease in sulphate aerosol formation through OH
10 oxidation because OH levels are decreased. The SO₂ not oxidised and not deposited is
11 transported downwind of the perturbed region, where it promotes sulphate aerosol formation
12 in the absence of oxidant limitation: in those regions, both models simulate negative aerosol
13 RFs. The balance between regions of positive and negative aerosol RF varies depending on
14 the model, the perturbed region, and the season. In contrast, OsloCTM2 does not simulate this
15 dipole of responses: its aerosol contribution is negative almost everywhere on the globe. The
16 representation of nitrate aerosols explains that difference of behaviour compared to the other
17 models. Nitrate exerts between 50 and 95% of R_F to NO_x perturbations in OsloCTM2,
18 with largest contributions in Northern Hemisphere winter months, adding a negative RF in,
19 and downwind of, the perturbed regions. This brings the total aerosol SRF firmly into
20 negative values.

21 **3.7 Volatile organic compounds**

22 Figure 9 shows globally- and annually-averaged SRF for volatile organic compound
23 perturbations in the three ECLIPSE models with tropospheric ozone chemistry schemes. Total
24 VOC SRF varies from $-0.53 \text{ mW m}^{-2} (\text{Tg}[\text{C}] \text{ yr}^{-1})^{-1}$ for the Europe Winter perturbation with
25 NorESM1 to $+2.07 \text{ mW m}^{-2} (\text{Tg}[\text{C}] \text{ yr}^{-1})^{-1}$ for the same perturbation with HadGEM3. So
26 models disagree on the sign of total VOC SRF, although it is generally positive. Qualitatively,
27 all models agree that ozone, methane, and primary-mode ozone contribute positive SRFs. So
28 the qualitative disagreement stems from the sign and magnitude of the aerosol contribution.
29 Methane and primary-mode ozone SRFs are computed as described in Sect. 3.6.



1 VOC chemistry is particularly complex and diverse. Decreasing VOC leads to a decrease in
2 their oxidation products, CO and O₃, therefore increasing OH and decreasing CH₄
3 concentrations (Lin et al., 1988). Different VOCs have different photochemical O₃ creation
4 potentials (Derwent et al., 2001). The three ECLIPSE models include a different number of
5 VOC species. The model with the largest number of VOC species is OsloCTM2, with 40
6 species: 28 in the tropospheric chemistry scheme and 12 in the secondary organic aerosol
7 scheme. Its broader range of VOC lifetimes and ozone production potentials means that it
8 simulates the strongest ozone SRF. HadGEM3 is at the other end of the range of species
9 considered and simulates the weakest ozone SRF. The models agree better in terms of
10 simulated patterns of ozone RF, which is mostly located in the latitude band of the perturbed
11 region (Figure S11).

12 Models disagree in the sign and strength of the aerosol contribution to VOC SRF. HadGEM3
13 simulated positive SRFs to all perturbations, except for East Asian Winter. Compared to the
14 ozone precursor perturbations discussed previously, which impact sulphate and nitrate
15 formation, VOC perturbations introduce a new way of perturbing aerosols, via secondary
16 organic aerosol formation. The strength of this link varies strongly between models because
17 of the heterogeneity in the number and type of VOC represented. Although HadGEM3 agrees
18 with NorESM1 and OsloCTM2 that aerosol RF is negative above the perturbed regions
19 (Figure S10), those negative RFs are weak and therefore easily compensated on a global
20 average by noisy positive contributions in regions where the aerosol internal mixture has been
21 perturbed (e.g. north-western Russia, Indonesia, South America). Observational constraints on
22 such internal mixture perturbations are lacking, so it is not currently possible to assess the
23 realism of HadGEM3's response. Aerosol SRF in OsloCTM2 is weaker than that in
24 NorESM1. This is due to the representation of nitrate aerosols, which counteract part of the
25 RF exerted by changes in sulphate aerosols, but also to a weaker R_{Fac}i contribution.

26

27 **3.8 Carbon monoxide**

28 Figure 10 shows globally- and annually-averaged SRF for carbon monoxide perturbations in
29 the three ECLIPSE models with tropospheric ozone chemistry schemes. Total CO SRF varies
30 from +0.18 mW m⁻² (Tg[CO] yr⁻¹)⁻¹ for the Europe Summer perturbation with NorESM1 to



1 +0.26 mW m⁻² (Tg[CO] yr⁻¹)⁻¹ for the East Asia Summer perturbation with HadGEM3. There
2 are no strong differences in SRF between the different source regions. Seasonally however,
3 models suggest the increased methane contribution in Winter perturbations make those more
4 efficient at exerting an SRF than Summer perturbations. Models agree that East Asian
5 perturbations exert slightly stronger SRFs than European perturbations because of a stronger
6 SRF by ozone. East Asian ozone exerts a stronger RF per unit ozone burden because of higher
7 NO_x background in that region but also because it is closer to the Equator, where more
8 sunlight leads to a more active photochemistry (Berntsen et al. 2006). Qualitatively, all
9 models agree that ozone, methane, and primary-mode ozone contribute positive SRFs.
10 Aerosol RF is also positive in HadGEM3 and NorESM1, but is weakly negative in
11 OsloCTM2. Methane and primary-mode ozone SRFs are computed as described in Sect. 3.6.

12 The contributions by short-lived perturbations to ozone are in reasonable agreement among
13 the models, both from a global average (Figure 10) and pattern (Figure S13) point of view.
14 All models also agree that the methane SRF contribution is larger than that of short-lived
15 ozone changes. This is in contrast to the results for VOC (Sect. 3.7), where the ozone
16 contribution dominates, and stems from the fact that CO has a weaker ozone production
17 potential caused by slower reaction rates (e.g. Bowman (1995)).

18 Both NorESM1 and OsloCTM2 simulate relatively weak contributions of aerosols to CO
19 SRF. The contribution simulated by OsloCTM2 is negative because the positive RFs exerted
20 by sulphate and secondary organic aerosols are more than compensated by a negative RF by
21 nitrate aerosols. HadGEM3 simulates a relatively strong response of aerosols to CO
22 perturbations (Figure S12), but that is because biomass-burning emissions were also perturbed
23 in this model. NorESM1 and OsloCTM2 only perturbed fossil-fuel combustion emissions,
24 and the results suggest that links between CO and aerosols are stronger for biomass-burning
25 sources. However, other sources of diversity, including the representation of atmospheric
26 chemistry, could also explain the differences in behaviour between HadGEM3 and the other
27 participating models.

28



1 **3.9 Shipping sector**

2 Figure 11 shows globally- and annually-averaged SRF for all species (SO₂, BC, OC, CH₄,
3 NO_x, VOC, and CO) emitted by the shipping sector. ECHAM6 lacks a tropospheric ozone
4 chemistry scheme, and therefore only simulates the aerosol contribution, and diagnoses R_{Faci}
5 only. OsloCTM2 is the only model that includes BC-on-snow RF and that quantifies BC
6 semi-direct RF (see methods in Sect. 3.2). Total shipping SRF varies from $-6.7 \text{ mWm}^{-2} (\text{Tg yr}^{-1})^{-1}$
7 for the Summer perturbation by NorESM1 to $-1.47 \text{ mWm}^{-2} (\text{Tg yr}^{-1})^{-1}$ for the Winter
8 perturbation by ECHAM6. Models agree qualitatively that ozone contributes a positive SRF.
9 Aerosols provide a negative SRF. Methane and primary-mode ozone also contribute a
10 negative SRF, mainly driven by emissions of NO_x. The qualitative agreement for those
11 components is also good. Methane and primary-mode ozone SRFs are computed as described
12 in Sect. 3.6.

13 The SRF contributed by short-lived changes in ozone are in good agreement among models,
14 both in terms of global averages (Figure 11) and geographical patterns (Figure S16), with
15 maxima in the Tropics. ECLIPSE models may overestimate that contribution, however,
16 because they do not represent ship plumes but instead assume instantaneous dilution of
17 emissions over their grid boxes. This assumption is known to lead to an overestimate of ozone
18 production by NO_x (Paoli et al., 2011). BC-on-snow (see also Figure S15) and BC semi-direct
19 SRF, which are quantified from OsloCTM2 simulations as described in Sect. 3.2, are weak.
20 Methane SRF is a large contribution to shipping SRF because ships emit in pristine
21 environments, where ozone precursor emissions have a relatively larger impact than in
22 polluted regions.

23 Models agree that aerosols dominate shipping SRF, but disagree on the strength of that
24 contribution. The causes of the disagreement are a convolution of the disagreements listed
25 above for individual species: among those, different lifetimes, different strengths of R_{Faci},
26 and different treatment of the aerosol mixing state. Geographical patterns are similar among
27 models and reflect main shipping routes (Figure S14). NorESM1 shows a region of positive
28 aerosol RF in the Arctic, caused by the long-range transport of its long-lived BC. That model
29 overestimates BC Arctic concentrations in the Summer, however (Sect. 3.2), so the positive
30 RF region may not be realistic.

31



1 **4 Matrix of specific radiative forcing**

2 Section 3 described the results of the perturbation simulations for each NTCF and each
3 model. This section describes how those results can be summarised into a best estimate and
4 range, which are more useful for most applications. However, all global numbers are given in
5 Supplementary Materials, to allow users to make other choices in deriving a best estimate or
6 range.

7 For each regional and seasonal perturbation by an NTCF, best estimates of SRF are provided
8 for each RF mechanism: aerosols (sum of RF_{ari} and RF_{aci}), BC deposition on snow, BC
9 rapid adjustments to semi-direct effects, short-lived changes in tropospheric ozone
10 concentrations, methane, and primary-mode ozone. The best estimate on net SRF is the sum
11 of the best estimates of all RF mechanisms that are relevant to the NTCF considered. Inter-
12 model diversity is represented by an interval ranging from the weaker SRF, obtained by
13 adding the weaker estimates of all RF mechanisms, to the stronger SRF, obtained by adding
14 the stronger estimates of all RF mechanisms. Best estimates of RF of BC deposition on snow
15 and BC rapid adjustments from semi-direct effects are available from only one model, so are
16 also taken to represent high and low estimates. It is however important to note that the
17 statistics on BC adjustments from semi-direct effects are not robust and that it may in fact not
18 be significantly different from zero for the Winter perturbations, as discussed in Sect. 3.2.

19 It can be argued that models that fail to provide realistic simulations of key aspects of NTCF
20 distributions and RF mechanisms should be discarded. For example, Shindell et al. (2013)
21 screen the 10 models that participated in ACCMIP for their ability to reproduce observed total
22 AOD and its recent trend, leading to a reduction in inter-model diversity. Such a screening is
23 not applied here because models do not exhibit uniform skill at reproducing aerosol or ozone
24 distributions: a model that could be considered best in one region often shows poorer skill in
25 another.

26 Nevertheless, decisions are required here on the inclusion of models that do not diagnose
27 RF_{aci}, or simulate long BC lifetimes, or lack nitrate aerosols, or simulate complex aerosol-
28 chemistry responses. The decisions are:

29 - For RF_{aci}, ECHAM6 is not included in best estimates of aerosol SRF because it does not
30 diagnose aci, which according to the other models is an important, and indeed often dominant,



1 contribution of total aerosol RF. It is possible that RF_{aci} is in fact compensated by rapid
2 adjustments in cloud liquid water path (e.g. Christensen and Stevens, 2011), meaning that
3 ECLIPSE models overestimate the strength of aerosol SRF. However, there is currently no
4 evidence that such compensation happens on a global scale.

5 - For BC lifetimes, a possible decision would be to discount models with BC lifetimes longer
6 than about 4 days, which is the lifetime obtained by constraining BC mass concentration
7 profiles with aircraft observations (Wang et al., 2014b; Hodnebrog et al., 2014). That decision
8 would give more weight to the aerosol SRF simulated by ECHAM6 and HadGEM3.
9 However, comparisons to surface observations in the Arctic suggest that ECHAM6 and
10 HadGEM3 underestimate BC concentrations in that region (Sect. 3.2), perhaps because
11 aerosols do not stay long enough in the atmosphere to be transported to the Arctic in those
12 two models. Reconciling mixed conclusions from different indirect observational constraints
13 on lifetime is therefore warranted. In the meantime, no model is discounted in this study when
14 producing the best ECLIPSE model estimate and range of BC SRF. Still, the tendency of
15 models to put BC too high in the atmosphere needs to be kept in mind, as it leads to an
16 overestimated SRF.

17 - For nitrate, the descriptions of results for the SO₂ (Sect. 3.1) and ozone precursor
18 (Sect. 3.6—3.8) perturbations note the importance of co-variations in nitrate aerosols. Those
19 are only represented in OsloCTM2 but are crucial in that model in determining the strength,
20 and on occasions even the sign, of aerosol SRF. For that reason, it is decided here to add the
21 nitrate SRF simulated by OsloCTM2 to the aerosol SRF of the other models. This solution is
22 crude, as it is known that model diversity in simulating nitrate distributions is large (Myhre et
23 al., 2013b) and a correlation between sulphate and nitrate RF can be expected from their links
24 through ammonium. But in the absence of a solid understanding of those correlations, the
25 solution adopted here has the merit of simplicity and prevents misleading overcorrections.

26 - For aerosol-chemistry interactions, HadGEM3 simulates complex responses of aerosols to
27 ozone precursor perturbations. This is particularly true of VOC perturbations (Sect. 3.7),
28 where HadGEM3 simulates a positive SRF when NorESM1 and OsloCTM2 agree on a
29 negative contribution. At this stage, the realism of HadGEM3's response cannot be confirmed
30 by observations, but nor can it be challenged. It is decided for that reason to include



1 HadGEM3 in the best estimate and range of VOC, with the caveat that the model behaviour is
2 peculiar.

3 Figure 12 shows the resulting best SRF estimate for all perturbations. Best estimates for each
4 mechanism are shown in colour. Best estimates for the net SRF are shown as black bars, with
5 the range from weaker to stronger estimates represented as whiskers. The range for NH₃
6 perturbations, which have been quantified from one model only, is assumed to be a factor 2
7 (Sect. 3.4). Model diversity ranges are often sizeable, but rarely include zero, indicating that
8 models generally agree on the sign of the SRF of a given NTCF. SO₂, OC, NH₃, NO_x, and
9 shipping sector perturbations exert negative SRF. BC aerosols, methane and CO exert positive
10 SRF. The sign of the SRF exerted by VOC perturbations is less robust. Its best estimate is
11 positive, but models cannot agree on the sign and the diversity range is large. The sign of
12 VOC SRF depends on the strength and sign of aerosol responses, including secondary organic
13 aerosols.

14 Quantitatively, best estimates of BC SRF are the strongest of all NTCFs, even after
15 accounting for rapid adjustments from semi-direct effects. Aerosol SRFs are generally
16 stronger than ozone precursor SRFs, with the exception of NH₃ perturbations, which exert
17 weak SRF because of competition with ammonium sulphate aerosol formation and because
18 the diurnal cycle of nitrate aerosol formation is unfavourable to ari (Sect. 3.4). NO_x exerts the
19 strongest SRF of all ozone precursor perturbations, although VOC perturbations are
20 potentially as strong. Shipping SRF is strong because of strong contributions by aerosols and
21 methane.

22 The best estimates of this study are included in Table 1 for convenient comparison to previous
23 studies. This study suggests a revision towards stronger SRFs for SO₂ and OC perturbations
24 because of the inclusion of RFaci. In contrast, this study's BC SRF is not very different than
25 that derived by studies that consider ari only, because the inclusion of aci, deposition on
26 snow, and rapid adjustments from semi-direct effects contributes only a weakly positive, and
27 even at times negative, SRF. The BC SRF in this study is however several times weaker than
28 that proposed by Bond et al. (2013), primarily because modelled ari is not scaled up to correct
29 for perceived underestimations in absorbing aerosol optical depth. Such corrections have been
30 challenged by Wang et al. (2014a) and Samset et al. (2014), so caution is justified. For
31 methane and ozone precursor perturbation, the study agrees well with previous efforts in



1 estimating the methane contribution. The SRF exerted by short-lived perturbations to ozone
2 concentrations is generally revised upward. This study quantifies aerosol responses to ozone
3 precursor perturbations for the first time across multiple models. Aerosols contribute a
4 negative SRF to NO_x perturbations, positive to CO perturbations. The contribution of
5 aerosols to VOC SRF is negative in two models, but positive in another. Finally, the study
6 also singles out the shipping sector, finding that its SRF is negative and mostly contributed by
7 aerosols and methane.

8

9 **4.1 Seasonality**

10 For all perturbations, SRF best estimates are given for emission reductions applied in two
11 periods, May-Oct and Nov-Apr, which are labelled in Figure 12 Summer and Winter,
12 respectively, because emission perturbations are predominantly located in the Northern
13 Hemisphere. The seasonality of methane perturbations was not considered because the time of
14 emission becomes quickly irrelevant compared to the long residence time of methane in the
15 atmosphere. NorESM1, which implemented Summer and Winter methane perturbations,
16 confirms that seasonality of methane emissions has a small impact, making a 7% difference in
17 methane SRF.

18 For aerosol primary and precursor perturbations, which are largely located in the Northern
19 Hemisphere, Summer emission reductions exert strong SRFs because the RF mechanisms act
20 mostly on shortwave radiation. For RF_{ari}, anthropogenic aerosols are predominantly located
21 in the accumulation mode, at sizes which interact most efficiently with shortwave radiation.
22 For RF_{aci}, changes to cloud albedo operate in the shortwave spectrum only, although BC
23 semi-direct SRF has a longwave component. In addition to RF mechanisms, chemical
24 production and sinks (mainly from precipitation) also influence seasonality. SO₂ photolysis is
25 an example of a reaction favoured by higher, summertime, shortwave radiative fluxes.
26 Temperature is also a factor, especially in nitrate aerosol formation, which is favoured by
27 colder temperatures. This dependence explains the unusual seasonality of NH₃ perturbations,
28 which exert stronger SRFs in Winter perturbations for East Asian and on a global average.
29 The fact that European perturbations behave differently is linked to the lower sulphate aerosol



1 levels in Europe, reducing their ability to limit nitrate formation in both summer and winter
2 months.

3 The SRF of ozone precursor perturbations is exerted across both the shortwave and longwave
4 spectra, so its seasonality is not as strong as for aerosol perturbations and the details of ozone
5 formation pathways are important. Figure 12 shows that Winter NO_x perturbations exert
6 stronger SRFs, except for European perturbations. The seasonality of NO_x RF depends on the
7 level of cancellation between the positive ozone contribution and the negative methane
8 contribution. Derwent et al. (2008) found using a CTM that there are no simple relationships
9 that explain that competition, which also varies regionally. Our results replicate that
10 complexity. CO Winter perturbations are consistently stronger than Summer perturbations,
11 but differences are generally small. Finally, VOC perturbations may have a seasonality where
12 Summer perturbations are stronger than Winter perturbations, but model diversity is large so
13 the seasonality is uncertain.

14

15 **4.2 Latitudinal variations**

16 Figures 13a and 13b show best estimates and ranges of SRF for aerosols and ozone
17 precursors, respectively, across four latitude bands: 90N–60N, 60N–28N, 28N–28S, and
18 28S–90S. Those bands have been chosen to represent the Arctic, mid-latitudes, Tropics, and
19 Southern Hemisphere extratropical latitudes, respectively. The Southern Hemisphere is less
20 resolved than the Northern Hemisphere because anthropogenic emissions are predominantly
21 located in the latter. European emission perturbations are entirely located in the second band
22 (60N–28N). East Asian emission perturbations also include the northern portion of the third
23 band (28N–28S). RotW and shipping perturbations are located across all four bands, but
24 again with Northern Hemisphere emissions having more weight.

25 Latitudinal averaging of RF is done on the annual distributions shown as Supplementary
26 Figures. SRF is then computed by normalising by the globally-averaged emission change: so
27 for a given perturbation, both global and latitudinal SRFs share the same normalisation
28 factors. Annual distributions are however not available for methane RF and BC rapid
29 adjustments to semi-direct effects. Methane RF has been computed as a global average only
30 (see Sect. 3.5). It is assumed here to be uniformly distributed across globe, which is justified



1 on an annual basis by the well-mixed nature of methane. BC rapid adjustments are associated
2 with noisy distributions (see Sect. 3.2), so there is low confidence in the significance of
3 regional patterns. They are assumed here to follow the same latitudinal distribution of BC
4 RFari, which is justified by the close physical links between the two RF processes.

5 Figures 13 show that although SRF is typically stronger in the latitude band where the
6 emission perturbation is applied, it is not confined to that latitude band. This behaviour is
7 expected from atmospheric transport, and has been found previously in other modelling
8 studies (e.g. Shindell and Faluvegi, 2009). European aerosol and precursor perturbations
9 affect the Arctic in a sizeable way. The BC European and Global Winter perturbations may
10 even exert a stronger positive SRF in the Arctic than in mid-latitudes where the perturbations
11 are located, because of the added positive contribution of BC-on-snow RF. The SRF exerted
12 by East Asian perturbations is more confined to mid-latitudes, because atmospheric transport
13 preferentially advects the perturbations towards the Pacific Ocean rather than the Arctic,
14 especially in Winter perturbations (Figure S2).

15 Ozone precursor perturbations (Figure 13b) tend to be more diffuse than their aerosol
16 counterparts, in part because of the longer lifetime of ozone in ECLIPSE models (Table 5) but
17 also because perturbations to OH lifetime are more efficient in the Tropics (Berntsen et al.,
18 2006). SRF of ozone precursor perturbations are therefore strong in both Northern
19 Hemisphere mid-latitudes, where the perturbations are located, and the Tropics. For European
20 and East Asian perturbations, the Arctic is generally associated with weaker SRFs, except for
21 CO, which is associated with more spatially uniform SRFs because methane RF is the main
22 contributor. The SRF of shipping sector perturbations peaks in the Northern Hemisphere,
23 where most shipping lanes are located.

24

25 **5 Conclusion**

26 This study provides NTCF SRFs by using ECLIPSE model simulations by four general
27 circulation and chemistry-transport models: ECHAM6, HadGEM3, NorESM1, and
28 OsloCTM2. SRFs are given for eight NTCF, four regions or sectors, and six RF mechanisms.
29 The four regions are Europe, East Asia, global average, and the shipping sector. The eight
30 NTCFs or NTCF precursors are SO₂, BC, OC, NH₃, methane, NO_x, CO, and VOC. NH₃
31 perturbations were applied in OsloCTM2 only, which includes a representation of nitrate



1 aerosols. The six RF mechanisms are aerosols (both ari and aci), BC deposition on snow, BC
2 rapid adjustments from semi-direct effects, short-lived ozone changes, methane, and primary-
3 mode ozone. OsloCTM2 is the only model used to estimate BC deposition on snow and BC
4 rapid adjustments from semi-direct effects. ECHAM6 does not simulate ozone chemistry, so
5 does not provide SRFs for the last three RF mechanisms on the list.

6 Models generally agree on the sign of the total SRF of a given NTCF. The SRF exerted by
7 SO₂, OC, NH₃, NO_x, and shipping sector perturbations is negative. The SRF exerted by
8 methane and CO is positive. Models also agree that BC SRF is positive, but is weakened by
9 rapid adjustments from semi-direct effects. Models do not agree on the sign of VOC SRF,
10 although its best estimate is positive, because of diversity in the aerosol responses. Model
11 diversity has multiple and complex roots, but four important aspects stand out.

- 12 - Diversity in modelled NTCF lifetimes is large, with longest lifetimes being 1.5 to 2.5
13 times longer than the shortest lifetimes depending on NTCF. Differences in lifetime
14 affect both the reach of long-range transport and the reference baseline.
- 15 - The unperturbed baseline causes diversity for non-linear RF mechanisms, such as
16 RFaci and methane RF. It is also a common cause for regional differences in SRF.
- 17 - The number of species represented varies among models. Nitrate and secondary
18 aerosols modulate the strength of the SRF exerted by SO₂, NO_x, VOC, and CO
19 perturbations, but are not included in all models, causing potentially misleading results
20 in models where those aerosol species are absent. Models that include VOC emissions
21 also account for a different number and type of VOC species.
- 22 - Interactions between aerosols and chemistry, and particularly aerosol responses to
23 changes in the oxidising capacity of the atmosphere and secondary organic aerosol
24 formation, affect the strength, possibly even the sign, and the seasonality of SRF. The
25 strength of those interactions differs among models.

26 Harmonising modelling capabilities, and deriving observational constraints on modelled
27 lifetimes (e.g. Kristiansen et al., 2016) and responses of OH concentrations to chemistry
28 perturbations will be useful in reducing model diversity while also quantifying model skill at
29 simulating atmospheric composition with fidelity. Other causes of diversity include different
30 aerosol optical properties, including BC absorbing properties (e.g. Myhre et al., 2013b);
31 different vertical profiles (e.g. Samset et al., 2013); different cloud processes, which affect the



1 strength of RF_{aci} (e.g. Quaas et al., 2009); and host model considerations, such as the use of
2 different radiative transfer schemes (Stier et al., 2013) and different simulations of horizontal
3 and vertical cloud distributions.

4 Models agree well on the ranking of the SRF of the NTCF considered in this study, with SRF
5 exerted by aerosol perturbations being up to an order of magnitude stronger than methane and
6 ozone precursor perturbations. An exception to that observation is the SRF exerted by NH₃
7 perturbations, which is weakened by the diurnal cycle of nitrate aerosol formation and
8 competition from sulphate aerosols. In terms of best estimates, BC exerts the strongest SRF of
9 all aerosol and precursor perturbations, while NO_x exerts the strongest SRFs of ozone
10 precursor perturbations, although VOC SRF may be as strong. Shipping sector SRF, which
11 combines strong contributions from aerosols and methane, is relatively strongly negative.
12 However, in terms of climate mitigation, this ranking of NTCF SRF should be understood in
13 the context of their individual emission rates. For example, although the BC SRF is about 20
14 times stronger on a global average than that of methane, the anthropogenic emission rate of
15 methane is 200 times larger. The negative RF obtained by the same relative change in
16 emission rates would therefore be stronger for methane than for BC.

17 Regionally, European aerosol perturbations exert stronger SRF than East Asian perturbations,
18 because East Asia has a more polluted baseline which saturates RF_{aci} and dampens the
19 impact of emission reductions. The regional dependence of ozone precursor SRF is more
20 complex, and no systematic rule is found, in common to previous studies (Derwent et al.,
21 2008). The strong aerosol and methane RF exerted by shipping perturbations are likely due to
22 emitting in pristine environments. SRF has an unequal latitudinal distribution, generally
23 peaking in the latitude band where the perturbation is applied, although other regions, notably
24 the Arctic, are affected through changes in transported NTCFs. In that respect, BC Winter
25 perturbations are notable for exerting stronger positive SRF in the Arctic than in Europe
26 because of the added contribution of BC-on-snow RF.

27 Seasonally, RF mechanisms that act primarily on shortwave radiation, such as aerosol ari and
28 aci, make the SRF of Summer perturbations stronger than that of Winter perturbations.
29 However, that seasonality may be inverted for species, such as nitrate aerosols, for which
30 chemical production has itself a strong seasonal dependence. Seasonality of ozone precursor
31 perturbations is more complex and region-dependent, but also less pronounced than for



1 aerosols. NorESM1 simulations found that the seasonality of methane SRF is weak, as
2 expected from a relatively long-lived NTCTF.

3 Ideally, the SRF matrix presented here should include rapid adjustments to all RF
4 mechanisms and be a matrix of specific ERF. But quantifying ERF is more challenging than
5 the already challenging task of quantifying RF, especially for the small regional and seasonal
6 perturbations considered here. The challenge is to distinguish, in a statistically robust way,
7 rapid adjustments from internal variability. The only rapid adjustment considered in this study
8 is from the semi-direct effect of BC aerosols, and the statistics are fragile. Nudging of
9 temperature and wind speeds have shown promise in decreasing the size of internal variability
10 (Kooperman et al., 2012), but whether that method also suppresses rapid adjustments is
11 unknown. One possible variation of that method is to allow temperature to adjust freely to
12 semi-direct effects, while wind speeds remain nudged to decrease internal variability between
13 perturbed and unperturbed simulations. Implemented in HadGEM3, that method successfully
14 reproduces the globally-averaged seasonality of ERF and subsequent precipitation changes
15 simulated by free-running simulations (Figures S17 and S18). The simulations required to do
16 so are 6 times shorter and have better statistics. This encouraging result holds for a variety of
17 RF mechanisms, including a doubling of carbon dioxide concentrations and RF ari and aci.
18 That method assumes that thermodynamical and dynamical responses are separated, at least
19 over rapid adjustment timescales. Whether that assumption is true and allows ERF to be
20 quantified confidently remains to be demonstrated.

21

22 **Data availability**

23 Supplementary Materials include spreadsheets giving all globally-averaged numbers for all
24 perturbation simulations and all radiative forcing mechanisms, by all models.

25

26 **Acknowledgements**

27 The research and simulations described in this study were funded by the European Union
28 Seventh Framework Programme (FP7/2007-2013) under grant agreement no 282688 –
29 ECLIPSE. The research team based at the University of Reading acknowledges use of the
30 MONSooN supercomputing system, a collaborative facility supplied under the Joint Weather



1 and Climate Research Programme, which is a strategic partnership between the UK Met
2 Office and the UK Natural Environment Research Council. The University of Leipzig team
3 acknowledges additional funding by the European Research Council (QUAERERE,
4 GA 306284) and computing time from the German Climate Computing Centre (DKRZ). The
5 CICERO team acknowledges additional funding from the Research Council of Norway
6 through the NetBC (no. 244141) and SLAC (no. 208277) projects.

7

8 **Author contribution**

9 N. Bellouin, G. Myhre, and J. Quaas designed the experiments as part of the ECLIPSE
10 project. N. Bellouin, L. Baker, Ø. Hodnebrog, D. Olivié, R. Cherian, C. Macintosh, B.
11 Samset, and A. Esteve ran the experiments or radiative transfer calculations, and analysed the
12 data sets. B. Aamaas provided additional data analysis in the perspective of climate metrics
13 users. N. Bellouin prepared the manuscript with contributions from all co-authors.

14

15 **References**

16 Aamaas, B., Berntsen, T. K., Fuglestedt, J. S., Shine, K. P., and Bellouin, N.: Multimodel
17 emission metrics for regional emissions of short lived climate forcers, *Atmos. Chem. Phys.*
18 *Discuss.*, 15, 26089-26130, doi:10.5194/acpd-15-26089-2015, 2015.

19 Baker, L. H., Collins, W. J., Olivié, D. J. L., Cherian, R., Hodnebrog, Ø., Myhre, G., and
20 Quaas, J.: Climate responses to anthropogenic emissions of short-lived climate pollutants,
21 *Atmos. Chem. Phys.*, 15, 8201-8216, doi:10.5194/acp-15-8201-2015, 2015a.

22 Bellouin, N., Rae, J., Jones, A., Johnson, C., Haywood, J., and Boucher, O.: Aerosol forcing
23 in the Climate Model Intercomparison Project (CMIP5) simulations by HadGEM2-ES and the
24 role of ammonium nitrate. *J. Geophys. Res.*, 116, D20206, doi:10.1029/2011JD016074, 2011.

25 Berntsen, T., Fuglestedt, J., Myhre, G., Stordal, F., and Berglen T.F.: Abatement of
26 Greenhouse Gases: Does Location Matter? *Climatic Change*, 74, 4, 377—411,
27 doi:10.1007/s10584-006-0433-4, 2006.

28 Bentsen, M., Bethke, I., Debernard, J. B., Iversen, T., Kirkevåg, A., Seland, Ø., Drange, H.,
29 Roelandt, C., Seierstad, I. A., Hoose, C., and Kristjánsson, J. E.: The Norwegian Earth



- 1 System Model, NorESM1-M – Part 1: Description and basic evaluation of the physical
2 climate, *Geosci. Model Dev.*, 6, 687–720, doi:10.5194/gmd-6-687-2013, 2013.
- 3 Bond, T. C. and Bergstrom, R. W.: Light absorption by carbonaceous particles: An
4 investigative review, *Aerosol Sci. Technol.*, 40, 27–67, doi:10.1080/02786820500421521,
5 2006.
- 6 Bond, T.C., S.J. Doherty, D.W. Fahey, P.M. Forster, T. Berntsen, B.J. DeAngelo, M.G.
7 Flanner, S. Ghan, B. Kärcher, D. Koch, S. Kinne, Y. Kondo, P.K. Quinn, M.C. Sarofim, M.G.
8 Schultz, M. Schulz, C. Venkataraman, H. Zhang, S. Zhang, N. Bellouin, S.K. Guttikunda,
9 P.K. Hopke, M.Z. Jacobson, J.W. Kaiser, Z. Klimont, U. Lohmann, J.P. Schwarz, D. Shindell,
10 T. Storelvmo, S.G. Warren, and C.S. Zender. Bounding the role of black carbon in the climate
11 system: A scientific assessment. *J. Geophys. Res.*, 118, 5380-5552, doi:10.1002/jgrd.50171,
12 2013.
- 13 Bowman, F.M.: A multi-parent assignment method for analyzing atmospheric chemistry
14 mechanisms. *Atmos. Environ.*, 39, 14, 2519—2533, doi:10.1016/j.atmosenv.2004.12.040,
15 2005.
- 16 Brioude, J., Cooper, O. R., Feingold, G., Trainer, M., Freitas, S. R., Kowal, D., Ayers, J.K.,
17 Prins, E., Minnis, P., McKeen, S. A., Frost, G. J., and Hsie, E.-Y.: Effect of biomass burning
18 on marine stratocumulus clouds off the California coast, *Atmos. Chem. Phys.*, 9, 8841-8856,
19 doi:10.5194/acp-9-8841-2009, 2009.
- 20 Carslaw, K.S., L.A. Lee, C.L. Reddington, K.J. Pringle, A. Rap, P.M. Forster, G.W. Mann,
21 D.V. Spracklen, M.T. Woodhouse, L.A. Regayre, and J.R. Pierce, Large contribution of
22 natural aerosols to uncertainty in indirect forcing, *Nature*, 503, 67–71,
23 doi:10.1038/nature12674, 2013.
- 24 Christensen, M.W., and Stephens, G.L.: Microphysical and macrophysical responses of
25 marine stratocumulus polluted by underlying ships: Evidence of cloud deepening, *J. Geophys.*
26 *Res.*, 116, D03201, doi:10.1029/2010JD014638, 2011.
- 27 Collins, W.D.: Parameterization of generalized cloud overlap for radiative calculations in
28 general circulation models, *J. Atmos. Sci.*, 58, 3224–3242, doi:10.1175/1520-0469(2001)058,
29 2001.



- 1 Dall'Osto, M., Harrison, R. M., Coe, H., Williams, P. I., and Allan, J. D.: Real time chemical
2 characterization of local and regional nitrate aerosols, *Atmos. Chem. Phys.*, 9, 3709-3720,
3 doi:10.5194/acp-9-3709-2009, 2009.
- 4 Dalsøren, S. B., Ø. Endresen, I. S. A. Isaksen, G. Gravir, and E. Sørsgård: Environmental
5 impacts of the expected increase in sea transportation, with a particular focus on oil and gas
6 scenarios for Norway and northwest Russia, *J. Geophys. Res.*, 112, D02310,
7 doi:10.1029/2005JD006927, 2007.
- 8 Derwent, R. G., Jenkin, M. E., Saunders, S. M., and Pilling, M. J.: Characterization of the
9 reactivities of volatile organic compounds using a master chemical mechanism, *J. Air Waste*
10 *Ma.*, 51, 5, 699-707, doi:10.1080/10473289.2001.10464297, 2001.
- 11 Derwent, R.G., D.S. Stevenson, R.M. Doherty, W.J. Collins, M.G. Sanderson, and C.E.
12 Johnson: Radiative forcing from surface NO_x emissions: spatial and seasonal variations,
13 *Climatic Change*, 88, 385—401, doi:10.1007/s10584-007-9383-8, 2008.
- 14 Dubovik, O., A. Smirnov, B. N. Holben, M. D. King, Y. J. Kaufman, T. F. Eck, and I.
15 Slutsker: Accuracy assessment of aerosol optical properties retrieval from AERONET sun
16 and sky radiance measurements. *J. Geophys. Res.*, 105, 9791–9806, 2000.
- 17 Eckhardt, S., Quennehen, B., Olivie, D. J. L., Berntsen, T. K., Cherian, R., Christensen, J. H.,
18 Collins, W., Crepinsek, S., Daskalakis, N., Flanner, M., Herber, A., Heyes, C., Hodnebrog,
19 Ø., Huang, L., Kanakidou, M., Klimont, Z., Langner, J., Law, K. S., Massling, A.,
20 Myriokefalitakis, S., Nielsen, I. E., Nøjgaard, J. K., Quaas, J., Quinn, P. K., Raut, J.-C.,
21 Rumbold, S. T., Schulz, M., Skeie, R. B., Skov, H., Lund, M. T., Uttal, T., von Salzen, K.,
22 Mahmood, R., and Stohl, A.: Current model capabilities for simulating black carbon and
23 sulfate concentrations in the Arctic atmosphere: a multi-model evaluation using a
24 comprehensive measurement data set, *Atmos. Chem. Phys. Discuss.*, 15, 10425-10477,
25 doi:10.5194/acpd-15-10425-2015, 2015.
- 26 Edwards, J. and Slingo, A.: Studies with a flexible new radiation code. I: Choosing a
27 configuration for a large-scale model, *Q. J. Roy. Meteor. Soc.*, 122, 689–719, 1996.
- 28 Emmons, L. K., Walters, S., Hess, P. G., Lamarque, J.-F., Pfister, G. G., Fillmore, D.,
29 Granier, C., Guenther, A., Kinnison, D., Laepple, T., Orlando, J., Tie, X., Tyndall, G.,
30 Wiedinmyer, C., Baughcum, S. L., and Kloster, S.: Description and evaluation of the Model



- 1 for Ozone and Related chemical Tracers, version 4 (MOZART-4), *Geosci. Model Dev.*, 3, 43–
2 67, doi:10.5194/gmd-3-43-2010, 2010.
- 3 Fujino, J., R. Nair, M. Kainuma, T. Masui, Y. Matsuoka: Multigas mitigation analysis on
4 stabilization scenarios using AIM global model. *The Energy Journal*, Special Issue 3, 343–
5 354, 2006.
- 6 Fuglestedt, Jan S., Keith P. Shine, Jolene Cook, Terje Berntsen, David S. Lee, Andrea
7 Stenke, Ragnhild Bieltvedt Skeie, Guus Velders and Ian Waitz: Transport Impacts on
8 Atmosphere and Climate: Metrics. *Atmospheric Environment*, 44, 4648-4677, 2010.
- 9 Gadhavi, H. S., Renuka, K., Ravi Kiran, V., Jayaraman, A., Stohl, A., Klimont, Z., and Beig,
10 G.: Evaluation of black carbon emission inventories using a Lagrangian dispersion model – a
11 case study over Southern India, *Atmos. Chem. Phys.*, 15, 1447–1461, doi:10.5194/acp-15-
12 1447-2015, 2015.
- 13 Ghan, S. J.: Technical Note: Estimating aerosol effects on cloud radiative forcing, *Atmos.*
14 *Chem. Phys.*, 13, 9971-9974, doi:10.5194/acp-13-9971-2013, 2013.
- 15 Hauglustaine, D. A., Balkanski, Y., and Schulz, M.: A global model simulation of present and
16 future nitrate aerosols and their direct radiative forcing of climate, *Atmos. Chem. Phys.*, 14,
17 11031-11063, doi:10.5194/acp-14-11031-2014, 2014.
- 18 Hegg, D. A.: Cloud condensation nucleus-sulphate mass relationship and cloud albedo, *J.*
19 *Geophys. Res.*, 99(D12), 25903–25907, doi:10.1029/94JD02224, 1994.
- 20 Hewitt, H. T., Copsey, D., Culverwell, I. D., Harris, C. M., Hill, R. S. R., Keen, A. B.,
21 McLaren, A. J., and Hunke, E. C.: Design and implementation of the infrastructure of
22 HadGEM3: the next-generation Met Office climate modelling system, *Geosci. Model Dev.*, 4,
23 223–253, doi:10.5194/gmd-4-223-2011, 2011.
- 24 Hodnebrog, Ø, G. Myhre, and B.H. Samset. How shorter black carbon lifetime alters its
25 climate effect. *Nature Communications*, 5, 5065, doi:10.1038/ncomms6065, 2014.
- 26 Holmes, C. D., M.J. Prather, O.A. Søvde, and G. Myhre: Future methane, hydroxyl, and their
27 uncertainties: key climate and emission parameters for future predictions, *Atmos. Chem.*
28 *Phys.*, 13, 285-302, doi:10.5194/acp-13-285-2013, 2013.



- 1 Iacono, M. J., J. S. Delamere, E. J. Mlawer, M. W. Shephard, S. A. Clough, and W. D.
2 Collins: Radiative forcing by long-lived greenhouse gases: Calculations with the AER
3 radiative transfer models, *J. Geophys. Res.*, 113, D13103, doi:10.1029/2008JD009944, 2008.
- 4 Iversen, T., Bentsen, M., Bethke, I., Debernard, J. B., Kirkevåg, A., Seland, Ø., Drange, H.,
5 Kristjansson, J. E., Medhaug, I., Sand, M., and Seierstad, I. A.: The Norwegian Earth System
6 Model, NorESM1-M – Part 2: Climate response and scenario projections, *Geosci. Model
7 Dev.*, 6, 389–415, doi:10.5194/gmd-6-389-2013, 2013.
- 8 Jiang, J. H., et al.: Evaluation of cloud and water vapor simulations in CMIP5 climate models
9 using NASA “A-Train” satellite observations, *J. Geophys. Res.*, 117, D14105,
10 doi:10.1029/2011JD017237, 2012.
- 11 Jiao, C., Flanner, M. G., Balkanski, Y., Bauer, S. E., Bellouin, N., Berntsen, T. K., Bian, H.,
12 Carslaw, K. S., Chin, M., De Luca, N., Diehl, T., Ghan, S. J., Iversen, T., Kirkevåg, A., Koch,
13 D., Liu, X., Mann, G. W., Penner, J. E., Pitari, G., Schulz, M., Seland, Ø., Skeie, R. B.,
14 Steenrod, S. D., Stier, P., Takemura, T., Tsigaridis, K., van Noije, T., Yun, Y., and Zhang, K.:
15 An AeroCom assessment of black carbon in Arctic snow and sea ice, *Atmos. Chem. Phys.*,
16 14, 2399–2417, doi:10.5194/acp-14-2399-2014, 2014.
- 17 Jones, A., Roberts, D. L., and Slingo, A. A climate model study of indirect radiative forcing
18 by anthropogenic sulphate aerosols. *Nature*, 370, 450–453, 1994.
- 19 Kirkevåg, A., Iversen, T., Seland, Ø., Hoose, C., Kristjánsson, J. E., Struthers, H., Ekman, A.
20 M. L., Ghan, S., Griesfeller, J., Nilsson, E. D., and Schulz, M.: Aerosol–climate interactions
21 in the Norwegian Earth System Model – NorESM1-M, *Geosci. Model Dev.*, 6, 207–244,
22 doi:10.5194/gmd-6-207-2013, 2013.
- 23 Koch, D. and Del Genio, A. D.: Black carbon semi-direct effects on cloud cover: review and
24 synthesis, *Atmos. Chem. Phys.*, 10, 7685–7696, doi:10.5194/acp-10-7685-2010, 2010.
- 25 Kooperman, G. J., M. S. Pritchard, S. J. Ghan, M. Wang, R. C. J. Somerville, and L. M.
26 Russell: Constraining the influence of natural variability to improve estimates of global
27 aerosol indirect effects in a nudged version of the Community Atmosphere Model 5,
28 *J. Geophys. Res.*, 117, D23204, doi:10.1029/2012JD018588, 2012.



- 1 Kristiansen, N.I., Stohl, A., and Wotawa, G.: Atmospheric removal times of the aerosol-
2 bound radionuclides ^{137}Cs and ^{131}I measured after the Fukushima Dai-ichi nuclear accident –
3 a constraint for air quality and climate models, *Atmos. Chem. Phys.*, 12, 10759–10769,
4 doi:10.5194/acp-12-10759-2012, 2012.
- 5 Kristiansen, N. I., Stohl, A., Olivie, D. J. L., Croft, B., Søvde, O. A., Klein, H., Christoudias,
6 T., Kunkel, D., Leadbetter, S. J., Lee, Y. H., Zhang, K., Tsigaridis, K., Bergman, T.,
7 Evangeliou, N., Wang, H., Ma, P.-L., Easter, R. C., Rasch, P. J., Liu, X., Pitari, G., Di
8 Genova, G., Zhao, S. Y., Balkanski, Y., Bauer, S. E., Faluvegi, G. S., Kokkola, H., Martin, R.
9 V., Pierce, J. R., Schulz, M., Shindell, D., Tost, H., and Zhang, H.: Evaluation of observed
10 and modelled aerosol lifetimes using radioactive tracers of opportunity and an ensemble of 19
11 global models, *Atmos. Chem. Phys.*, 16, 3525-3561, doi:10.5194/acp-16-3525-2016, 2016.
- 12 Lacis, A.A., D.J. Wuebbles, and J.A. Logan: Radiative forcing of climate by changes in the
13 vertical distribution of ozone, *J. Geophys. Res.*, 95, 9971-9981,
14 doi:10.1029/JD095iD07p09971, 1990.
- 15 Lamarque, J.-F., Bond, T. C., Eyring, V., Granier, C., Heil, A., Klimont, Z., Lee, D., Liousse,
16 C., Mieville, A., Owen, B., Schultz, M. G., Shindell, D., Smith, S. J., Stehfest, E., Van
17 Aardenne, J., Cooper, O. R., Kainuma, M., Mahowald, N., McConnell, J. R., Naik, V., Riahi,
18 K., and van Vuuren, D. P.: Historical (1850–2000) gridded anthropogenic and biomass
19 burning emissions of reactive gases and aerosols: methodology and application, *Atmos. Chem.*
20 *Phys.*, 10, 7017-7039, doi:10.5194/acp-10-7017-2010, 2010.
- 21 Lamarque, J.-F., Shindell, D. T., Josse, B., Young, P. J., Cionni, I., Eyring, V., Bergmann, D.,
22 Cameron-Smith, P., Collins, W. J., Doherty, R., Dalsoren, S., Faluvegi, G., Folberth, G.,
23 Ghan, S. J., Horowitz, L. W., Lee, Y. H., MacKenzie, I. A., Nagashima, T., Naik, V.,
24 Plummer, D., Righi, M., Rumbold, S. T., Schulz, M., Skeie, R. B., Stevenson, D. S., Strode,
25 S., Sudo, K., Szopa, S., Voulgarakis, A., and Zeng, G.: The Atmospheric Chemistry and
26 Climate Model Intercomparison Project (ACCMIP): overview and description of models,
27 simulations and climate diagnostics, *Geosci. Model Dev.*, 6, 179-206, doi:10.5194/gmd-6-
28 179-2013, 2013.
- 29 Lin, X., Trainer, M., and Liu, S. C.: On the nonlinearity of the tropospheric ozone production,
30 *J. Geophys. Res.*, 93(D12), 15879–15888, doi:10.1029/JD093iD12p15879, 1988.



- 1 Lohmann, U., Stier, P., Hoose, C., Ferrachat, S., Kloster, S., Roeckner, E., and Zhang, J.:
2 Cloud microphysics and aerosol indirect effects in the global climate model ECHAM5-HAM,
3 *Atmos. Chem. Phys.*, 7, 3425–3446, doi:10.5194/acp-7-3425-2007, 2007.
- 4 Mann, G. W., Carslaw, K. S., Spracklen, D. V., Ridley, D. A., Manktelow, P. T.,
5 Chipperfield, M. P., Pickering, S. J., and Johnson, C. E.: Description and evaluation of
6 GLOMAP-mode: a modal global aerosol microphysics model for the UKCA composition-
7 climate model, *Geosci. Model Dev.*, 3, 519–551, doi:10.5194/gmd-3-519-2010, 2010.
- 8 Metzger, S., F. Dentener, S. Pandis, and J. Lelieveld, Gas/aerosol partitioning, 1, A
9 computationally efficient model, *J. Geophys. Res.*, 107, D16, doi:10.1029/2001JD001102,
10 2002.
- 11 Myhre, G., E.J. Highwood, K.P. Shine, and F. Stordal: New estimates of radiative forcing due
12 to well mixed greenhouse gases, *Geophys. Res. Lett.*, 25, 14, 2715-2718,
13 doi:10.1029/98GL01908, 1998.
- 14 Myhre, G., Karlsdottir, S., Isaksen, I. S. A., and Stordal, F.: Radiative forcing due to changes
15 in tropospheric ozone in the period 1980 to 1996, *J. Geophys. Res.*, 105, 28935–28942, 2000.
- 16 Myhre, G., Bellouin, N., Berglen, T. F., Berntsen, T. K., Boucher, O., Grini, A., Isaksen, I. S.
17 A., Johnsrud, M., Mishchenko, M. I., Stordal, F., and Tanre, D.: Comparison of the radiative
18 properties and direct radiative effect of aerosols from a global aerosol model and remote
19 sensing data over ocean, *Tellus B*, 59, 115–129, 2007a.
- 20 Myhre, G., J. S. Nilsen, L. Gulstad, K. P. Shine, B. Rognerud, and I. S. A. Isaksen, Radiative
21 forcing due to stratospheric water vapour from CH₄ oxidation, *Geophys. Res. Lett.*, 34,
22 L01807, doi:10.1029/2006GL027472, 2007b.
- 23 Myhre, G., Berglen, T. F., Johnsrud, M., Hoyle, C. R., Berntsen, T. K., Christopher, S. A.,
24 Fahey, D. W., Isaksen, I. S. A., Jones, T. A., Kahn, R. A., Loeb, N., Quinn, P., Remer, L.,
25 Schwarz, J. P., and Yttri, K. E.: Modelled radiative forcing of the direct aerosol effect with
26 multi-observation evaluation, *Atmos. Chem. Phys.*, 9, 4, 1365-1392, 10.5194/acp-9-1365-
27 2009, 2009.
- 28 Myhre, G., D. Shindell, F.-M. Bréon, W. Collins, J. Fuglestedt, J. Huang, D. Koch, J.-F.
29 Lamarque, D. Lee, B. Mendoza, T. Nakajima, A. Robock, G. Stephens, T. Takemura and H.



- 1 Zhang: Anthropogenic and Natural Radiative Forcing. In: Climate Change 2013: The Physical
2 Science Basis. Contribution of Working Group I to the Fifth Assessment Report of the
3 Intergovernmental Panel on Climate Change [Stocker, T.F., D. Qin, G.-K. Plattner, M.
4 Tignor, S.K. Allen, J. Boschung, A. Nauels, Y. Xia, V. Bex and P.M. Midgley (eds.)].
5 Cambridge University Press, Cambridge, United Kingdom and New York, NY, USA, 2013a.
- 6 Myhre, G., B.H. Samset, M. Schulz, Y. Balkanski, S. Bauer, T.K. Berntsen, H. Bian, N.
7 Bellouin, M. Chin, T. Diehl, R.C. Easter, J. Feichter, S.J. Ghan, D. Hauglustaine, T. Iversen,
8 S. Kinne, A. Kirkevåg, J.-F. Lamarque, G. Lin, X. Liu, M.T. Lund, G. Luo, X. Ma, T. van
9 Noije, J. E. Penner, P.J. Rasch, A. Ruiz, Ø. Seland, R.B. Skeie, P. Stier, T. Takemura, K.
10 Tsigaridis, P. Wang, Z. Wang, L. Xu, H. Yu, F. Yu, J.-H. Yoon, K. Zhang, H. Zhang, and C.
11 Zhou.: Radiative forcing of the direct aerosol effect from AeroCom Phase II simulations.
12 *Atmos. Chem. Phys.*, 13, 1853-1877, doi:10.5194/acp-13-1853-2013, 2013b.
- 13 Neale, R.B., *et al.*, Description of the NCAR Community Atmosphere Model (CAM 4.0),
14 NCAR Technical Report, NCAR/TN-485+STR, National Center for Atmospheric Research
15 (NCAR), Boulder, Colorado, 2010.
- 16 O'Connor, F. M., Johnson, C. E., Morgenstern, O., Abraham, N. L., Braesicke, P., Dalvi, M.,
17 Folberth, G. A., Sanderson, M. G., Telford, P. J., Voulgarakis, A., Young, P. J., Zeng, G.,
18 Collins, W. J., and Pyle, J. A.: Evaluation of the new UKCA climate-composition model –
19 Part 2: The Troposphere, *Geosci. Model Dev.*, 7, 41–91, doi:10.5194/gmd-7-41-2014, 2014.
- 20 Paoli, R., Cariolle, D., and Sausen, R.: Review of effective emissions modeling and
21 computation, *Geosci. Model Dev.*, 4, 643–667, doi:10.5194/gmd-4-643-2011, 2011.
- 22 Prather, M.J. Time scales in atmospheric chemistry: Theory, GWPs for CH₄ and CO, and
23 runaway growth, *Geophys. Res. Lett.*, 23, 19, 2597–2600, doi:10.1029/96GL02371, 1996.
- 24 Quaas, J., Y. Ming, S. Menon, T. Takemura, M. Wang, J.E. Penner, A. Gettelman, U.
25 Lohmann, N. Bellouin, O. Boucher, A.M. Sayer, G.E. Thomas, A. McComiskey, G. Feingold,
26 C. Hoose, J.E. Kristjansson, X. Liu, Y. Balkanski, L.J. Donner, P.A. Ginoux, P. Stier, B.
27 Grandey, J. Feichter, I. Sednev, S.E. Bauer, D. Koch, R.G. Grainger, A. Kirkevåg, T. Iversen,
28 Ø. Seland, R. Easter, S.J. Ghan, P.J. Rasch, H. Morrison, J.-F. Lamarque, M.J. Iacono, S.
29 Kinne, and M. Schulz. Aerosol indirect effects - general circulation model intercomparison
30 and evaluation with satellite data. *Atmos. Chem. Phys.*, 9, 8697-8717, 2009.



- 1 Quennehen, B., Raut, J.-C., Law, K. S., Ancellet, G., Clerbaux, C., Kim, S.-W., Lund, M. T.,
2 Myhre, G., Olivieri, D. J. L., Safieddine, S., Skeie, R. B., Thomas, J. L., Tsyro, S., Bazureau,
3 A., Bellouin, N., Daskalakis, N., Hu, M., Kanakidou, M., Klimont, Z., Kupiainen, K.,
4 Myriokefalitakis, S., Quaas, J., Rumbold, S. T., Schulz, M., Cherian, R., Shimizu, A., Wang,
5 J., Yoon, S.-C., and Zhu, T.: Multi-model evaluation of short-lived pollutant distributions
6 over East Asia during summer 2008, *Atmos. Chem. Phys. Discuss.*, 15, 11049-11109,
7 doi:10.5194/acpd-15-11049-2015, 2015.
- 8 Randles, C. A., Kinne, S., Myhre, G., Schulz, M., Stier, P., Fischer, J., Doppler, L.,
9 Highwood, E., Ryder, C., Harris, B., Huttunen, J., Ma, Y., Pinker, R. T., Mayer, B.,
10 Neubauer, D., Hitzenberger, R., Oreopoulos, L., Lee, D., Pitari, G., Di Genova, G., Quaas, J.,
11 Rose, F. G., Kato, S., Rumbold, S. T., Vardavas, I., Hatzianastassiou, N., Matsoukas, C.,
12 Yu, H., Zhang, F., Zhang, H., and Lu, P.: Intercomparison of shortwave radiative transfer
13 schemes in global aerosol modeling: results from the AeroCom Radiative Transfer
14 Experiment, *Atmos. Chem. Phys.*, 13, 2347–2379, doi:10.5194/acp-13-2347-2013, 2013.
- 15 Riahi, K., Gruebler, A., and Nakicenovic, N.: Scenarios of long-term socio-economic and
16 environmental development under climate stabilization, *Technol. Forecast. Soc. Change*, 74,
17 887–935, 2007.
- 18 Saleh, R., Robinson, E.S., Tkacik, D.S., Ahern, A.T., Liu, S., Aiken, A.C., Sullivan, R.C.,
19 Presto, A.A., Dubey, M.K., Yokelson, R.J., Donahue, N.M., Robinson, A.L.: Brownness of
20 organics in aerosols from biomass burning linked to their black carbon content, *Nature*
21 *Geoscience*, 7, 647–650, doi:10.1038/ngeo2220, 2014.
- 22 Samset, B.H., G. Myhre, M. Schulz, Y. Balkanski, S. Bauer, T.K. Berntsen, H. Bian, N.
23 Bellouin, T. Diehl, R.C. Easter, S.J. Ghan, T. Iversen, S. Kinne, A. Kirkevåg, J.-F. Lamarque,
24 G. Lin, X. Liu, J.E. Penner, Ø. Seland, R.B. Skeie, P. Stier, T. Takemura, K. Tsigaridis, and
25 K. Zhang. Black carbon vertical profiles strongly affect its radiative forcing uncertainty.
26 *Atmos. Chem. Phys.*, 13, 2423-2434, doi:10.5194/acp-13-2423-2013, 2013.
- 27 Samset, B. H., Myhre, G., Herber, A., Kondo, Y., Li, S.-M., Moteki, N., Koike, M.,
28 Oshima, N., Schwarz, J. P., Balkanski, Y., Bauer, S. E., Bellouin, N., Berntsen, T. K.,
29 Bian, H., Chin, M., Diehl, T., Easter, R. C., Ghan, S. J., Iversen, T., Kirkevåg, A.,
30 Lamarque, J.-F., Lin, G., Liu, X., Penner, J. E., Schulz, M., Seland, Ø., Skeie, R. B., Stier, P.,



- 1 Takemura, T., Tsigaridis, K., and Zhang, K.: Modelled black carbon radiative forcing and
2 atmospheric lifetime in AeroCom Phase II constrained by aircraft observations, *Atmos. Chem.*
3 *Phys.*, 14, 12465-12477, doi:10.5194/acp-14-12465-2014, 2014.
- 4 Schulz, M., Olivie, D., Tsyro, S., Kanakidou, M., Myriokefalitakis, S., Daskalakis, N., Im, U.,
5 Fanourgakis, G., Hodnebrog, Ø., Skeie, R., Lund, M., Myhre, G., Bellouin, N., Rumbold, S.,
6 Collins, B., Cherian, R., and Quaas, J.: ECLIPSE Deliverable 2.1: Report on model accuracy,
7 available from <http://eclipse.nilu.no/language/en-GB/ProjectOverview/Deliverables.aspx>,
8 2015.
- 9 Shindell, D., and G. Faluvegi: Climate response to regional radiative forcing during the
10 twentieth century, *Nature Geosci.*, 2, 294-300, doi:10.1038/ngeo473, 2009.
- 11 Shindell, D.T., G. Faluvegi, D.M. Koch, G.A. Schmidt, N. Unger, and S.E. Bauer: Improved
12 attribution of climate forcing to emissions. *Science*, 326, 716-718,
13 doi:10.1126/science.1174760, 2009.
- 14 Shindell, D. T., Lamarque, J.-F., Schulz, M., Flanner, M., Jiao, C., Chin, M., Young, P. J.,
15 Lee, Y. H., Rotstajn, L., Mahowald, N., Milly, G., Faluvegi, G., Balkanski, Y., Collins, W. J.,
16 Conley, A. J., Dalsoren, S., Easter, R., Ghan, S., Horowitz, L., Liu, X., Myhre, G.,
17 Nagashima, T., Naik, V., Rumbold, S. T., Skeie, R., Sudo, K., Szopa, S., Takemura, T.,
18 Voulgarakis, A., Yoon, J.-H., and Lo, F.: Radiative forcing in the ACCMIP historical and
19 future climate simulations, *Atmos. Chem. Phys.*, 13, 2939-2974, doi:10.5194/acp-13-2939-
20 2013, 2013.
- 21 Shindell, D.: Inhomogeneous forcing and transient climate sensitivity. *Nature Climate*
22 *Change*, 4, 274-277, doi:10.1038/nclimate2136, 2014.
- 23 Shine, K.P., Fuglestedt, J.S., Hailemariam, K., and Stuber, S.: Alternatives to the global
24 warming potential for comparing climate impacts of emissions of greenhouse gases, *Climatic*
25 *Change*, 68, 3, 281-302, doi:10.1007/s10584-005-1146-9, 2005.
- 26 Skeie, R. B., Berntsen, T. K., Myhre, G., Tanaka, K., Kvalevåg, M. M., and Hoyle, C. R.:
27 Anthropogenic radiative forcing time series from pre-industrial times until 2010, *Atmos.*
28 *Chem. Phys.*, 11, 11827-11857, doi:10.5194/acp-11-11827-2011, 2011.



- 1 Smith, S.J., Karas, J., Edmonds, J., Eom, J., and Mizrahi, A.: Sensitivity of multi-gas climate
2 policy to emission metrics, *Climatic Change*, 117, 4, 663-675, doi:10.1007/s10584-012-0565-
3 7, 2013.
- 4 Stevens, B., and Feingold, G. Untangling aerosol effects on clouds and precipitation in a
5 buffered system, *Nature*, 461, 607-613, doi:10.1038/nature08281, 2009.
- 6 Stevens, B., Giorgetta, M., Esch, M., Mauritsen, T., Crueger, T., Rast, S., Salzmann, M.,
7 Schmidt, H., Bader, J., Block, K., Brokopf, R., Fast, I., Kinne, S., Kornblueh, L., Lohmann,
8 U., Pincus, R., Reichler, T., and Roeckner, E.: Atmospheric component of the MPI-M Earth
9 System Model: ECHAM6, *J. Adv. Model. Earth Sy.*, 5, 146–172, 2013.
- 10 Stevenson, D.S., P.J. Young, V. Naik, J.-F. Lamarque, D.T. Shindell, A. Voulgarakis, R.B.
11 Skeie, S.B. Dalsoren, G. Myhre, T.K. Berntsen, G.A. Folberth, S.T. Rumbold, W.J. Collins,
12 I.A. MacKenzie, R.M. Doherty, G. Zeng, T.P.C. van Noije, A. Strunk, D. Bergmann, P.
13 Cameron-Smith, D.A. Plummer, S.A. Strode, L. Horowitz, Y.H. Lee, S. Szopa, K. Sudo, T.
14 Nagashima, B. Josse, I. Cionni, M. Righi, V. Eyring, A. Conley, K.W. Bowman, and O. Wild:
15 Tropospheric ozone changes, radiative forcing and attribution to emissions in the
16 Atmospheric Chemistry and Climate Model Inter-comparison Project (ACCMIP). *Atmos.*
17 *Chem. Phys.*, **13**, 3063-3085, doi:10.5194/acp-13-3063-2013, 2013.
- 18 Stier, P., Feichter, J., Kinne, S., Kloster, S., Vignati, E., Wilson, J., Ganzeveld, L., Tegen, I.,
19 Werner, M., Balkanski, Y., Schulz, M., Boucher, O., Minikin, A., and Petzold, A.: The
20 aerosol-climate model ECHAM5-HAM, *Atmos. Chem. Phys.*, 5, 1125–1156, doi:10.5194/acp-
21 5-1125-2005, 2005.
- 22 Stier, P., N.A.J. Schutgens, N. Bellouin, H. Bian, O. Boucher, M. Chin, S. Ghan, N. Huneeus,
23 S. Kinne, G. Lin, X. Ma, G. Myhre, J.E. Penner, C.A. Randles, B. Samset, M. Schulz, T.
24 Takemura, F. Yu, H. Yu, and C. Zhou. Host model uncertainties in aerosol radiative forcing
25 estimates: results from the AeroCom Prescribed intercomparison study. *Atmos. Chem. Phys.*,
26 13, 3245-3270, doi:10.5194/acp-13-3245-2013, 2013.
- 27 Stohl, A., Aamaas, B., Amann, M., Baker, L. H., Bellouin, N., Berntsen, T. K., Boucher, O.,
28 Cherian, R., Collins, W., Daskalakis, N., Dusinska, M., Eckhardt, S., Fuglestedt, J. S., Harju,
29 M., Heyes, C., Hodnebrog, Ø., Hao, J., Im, U., Kanakidou, M., Klimont, Z., Kupiainen, K.,
30 Law, K. S., Lund, M. T., Maas, R., MacIntosh, C. R., Myhre, G., Myriokefalitakis, S., Olivie,



- 1 D., Quaas, J., Quennehen, B., Raut, J.-C., Rumbold, S. T., Samset, B. H., Schulz, M., Seland,
2 Ø., Shine, K. P., Skeie, R. B., Wang, S., Yttri, K. E., and Zhu, T.: Evaluating the climate and
3 air quality impacts of short-lived pollutants, *Atmos. Chem. Phys. Discuss.*, 15, 15155-15241,
4 doi:10.5194/acpd-15-15155-2015, 2015.
- 5 Streets, D. G., et al.: An inventory of gaseous and primary aerosol emissions in Asia in the
6 year 2000. *J. Geophys. Res.*, 108, 8809, doi:10.1029/2002JD003093, D21, 2003.
- 7 Taylor, J.P. and A. McHaffie: Measurements of cloud susceptibility, *J. Atmos. Sci.*, 51, 10,
8 1298—1306, 1994.
- 9 Tsigaridis, K., Daskalakis, N., Kanakidou, M., Adams, P. J., Artaxo, P., Bahadur, R.,
10 Balkanski, Y., Bauer, S. E., Bellouin, N., Benedetti, A., Bergman, T., Berntsen, T. K.,
11 Beukes, J. P., Bian, H., Carslaw, K. S., Chin, M., Curci, G., Diehl, T., Easter, R. C., Ghan, S.
12 J., Gong, S. L., Hodzic, A., Hoyle, C. R., Iversen, T., Jathar, S., Jimenez, J. L., Kaiser, J. W.,
13 Kirkevåg, A., Koch, D., Kokkola, H., Lee, Y. H., Lin, G., Liu, X., Luo, G., Ma, X., Mann, G.
14 W., Mihalopoulos, N., Morcrette, J.-J., Müller, J.-F., Myhre, G., Myriokefalitakis, S., Ng, N.
15 L., O'Donnell, D., Penner, J. E., Pozzoli, L., Pringle, K. J., Russell, L. M., Schulz, M., Sciare,
16 J., Seland, Ø., Shindell, D. T., Sillman, S., Skeie, R. B., Spracklen, D., Stavrakou, T.,
17 Steenrod, S. D., Takemura, T., Tiitta, P., Tilmes, S., Tost, H., van Noije, T., van Zyl, P. G.,
18 von Salzen, K., Yu, F., Wang, Z., Wang, Z., Zaveri, R. A., Zhang, H., Zhang, K., Zhang, Q.,
19 and Zhang, X.: The AeroCom evaluation and intercomparison of organic aerosol in global
20 models, *Atmos. Chem. Phys.*, 14, 10845-10895, doi:10.5194/acp-14-10845-2014, 2014.
- 21 Vignati, E., Wilson, J., and Stier, P.: M7: an efficient size-resolved aerosol microphysics
22 module for large-scale aerosol transport models, *J. Geophys. Res.*, 109, D22202,
23 doi:10.1029/2003JD004485, 2004.
- 24 Wang, X., Heald, C. L., Ridley, D. A., Schwarz, J. P., Spackman, J. R., Perring, A. E.,
25 Coe, H., Liu, D., and Clarke, A. D.: Exploiting simultaneous observational constraints on
26 mass and absorption to estimate the global direct radiative forcing of black carbon and brown
27 carbon, *Atmos. Chem. Phys.*, 14, 10989-11010, doi:10.5194/acp-14-10989-2014, 2014a.
- 28 Wang, Q. Q., D.J. Jacob, J.R. Spackman, A.R. Perring, J.P. Schwartz, N. Moteki, E.A.
29 Marais, C. Ge, J. Wang, and S.R.H. Barrett: Global budget and radiative forcing of black



- 1 carbon aerosol: Constraints from pole-to-pole (HIPPO) observations across the Pacific, *J.*
2 *Geophys. Res.*, 119, 195–206, doi:10.1002/2013JD020824, 2014b.
- 3 Wang, R., Y. Balkanski, O. Boucher, P. Ciais, G. L. Schuster, F. Chevallier, B. H. Samset, J.
4 Liu, S. Piao, M. Valari, S. Tao, Quantifying the role of black carbon in the Earth's climate
5 system, *Nature Scientific Reports*, submitted, 2015.
- 6 Wilcox, E. M.: Stratocumulus cloud thickening beneath layers of absorbing smoke aerosol,
7 *Atmos. Chem. Phys.*, 10, 11769–11777, doi:10.5194/acp-10-11769-2010, 2010.
- 8 Wilcox, L. J., Highwood, E. J., Booth, B. B. B. and Carslaw, K. S.: Quantifying sources of
9 inter-model diversity in the cloud albedo effect. *Geophys. Res. Lett.*, 42: 1568–1575. doi:
10 10.1002/2015GL063301, 2015.
- 11 WMO: Scientific Assessment of Ozone Depletion: 2014, Global Ozone Research and
12 Monitoring Project - Report No. 55, World Meteorological Organization, Geneva,
13 Switzerland, 2014.
- 14 Yu, H., M. Chin, J.J West, C.S. Atherton, N. Bellouin, D. Bergmann, I. Bey, H. Bian, T.
15 Diehl, G. Forberth, P. Hess, M. Schulz, D. Shindell, T. Takemura, and Q. Tan. A multimodel
16 assessment of the influence of regional anthropogenic emission reductions on aerosol direct
17 radiative forcing and the role of intercontinental transport. *J. Geophys. Res.*, 118, 700–720,
18 doi:10.1029/2012JD018148, 2013.
- 19 Zhang, K., O'Donnell, D., Kazil, J., Stier, P., Kinne, S., Lohmann, U., Ferrachat, S., Croft, B.,
20 Quaas, J., Wan, H., Rast, S., and Feichter, J.: The global aerosol-climate model ECHAM-
21 HAM, version 2: sensitivity to improvements in process representations, *Atmos. Chem. Phys.*,
22 12, 8911–8949, doi:10.5194/acp-12-8911-2012, 2012.
- 23


 1 **6 Tables**

2

3 **Table 1.** Specific radiative forcing (SRF), in $\text{mWm}^{-2} (\text{Tg yr}^{-1})^{-1}$, of near-term climate forcers,
 4 as estimated by scientific assessments and multi-model inter-comparisons. Numbers shown
 5 are median and full range for all studies, except for: - Bond et al. (2013), where best estimate
 6 and 90% confidence range are given; - Yu et al. (2013), where mean and standard deviation
 7 are given; - this study, where average and full range are given. Black Carbon (BC) and
 8 Organic Carbon (OC) aerosols are for fossil- and bio-fuel sources only, except for Bond et
 9 al. (2013) which also includes biomass-burning sources. For aerosols, the radiative forcing is
 10 for aerosol-radiation interactions (ari) only, except for the estimate by Bond et al. (2013)
 11 denoted “All”, which also includes aerosol-cloud and aerosol-surface interactions, and for
 12 estimates by this study, which also include aerosol-cloud interactions (aci).

Emitted compound	Climate Forcer	Reference	Method	SRF ($\text{mWm}^{-2} (\text{Tg yr}^{-1})^{-1}$)
SO ₂	SO ₄	Myhre et al. (2013b)	AeroCom, 15 models, ari only	-3.5 (-5.5 to -1.5)
		Shindell et al. (2013)	ACCMIIP, 9 models, ari only	-4.3 (-6.4 to -2.0)
		Yu et al. (2013)	HTAP, 8 models, 4 source regions, ari only	-2.9 ± 0.8 to -3.9 ± 0.8 depending on region
		<i>This study</i>	ECLIPSE, 3 models, 3 source regions, 2 seasons, ari +aci	-3.1 to -10.7 (-1.9 to -17.7) depending on region
OC	OC	Myhre et al. (2013b)	AeroCom, 15 models, ari only	-3.8 (-7.6 to -1.3)
		Shindell et al. (2013)	ACCMIIP, 4 models, ari only	-3.8 (-10.1 to -1.3)
		Yu et al. (2013)	HTAP, 8 models, 4 source regions, ari only	-3.7 ± 1.8 to -4.4 ± 1.7 depending on region
		<i>This study</i>	ECLIPSE, 3 models, 3 source regions, 2 seasons, ari +aci	-4.4 to -22.5 (+1.2 to -32.5) depending on region
BC	BC	Bond et al. (2013)	Assessment of models with observational constraints, ari only	+114.8 (+13.1 to +208.2)



		Bond et al. (2013)	Assessment of models with observational constraints, all RF mechanisms	+180.3 (+27.9 to +344.3)
		Myhre et al. (2013b)	AeroCom, 15 models, ari only	+45.3 (+15.1 to +75.6)
		Shindell et al. (2013)	ACCMIP, 5 models, ari only	+50.4 (+35.3 to +95.7)
		Yu et al. (2013)	HTAP, 8 models, 4 source regions, ari only	+25.3±14.6 to +37.4±19.3 depending on region
		<i>This study</i>	ECLIPSE, 4 models, 3 source regions, 2 seasons, ari+aci+deposition on snow and rapid adjustments from the semi-direct effect	+28.7 to +69.7 (+9.8 to +101.1) depending on region
NH ₃	NO ₃	Myhre et al. (2013b)	AeroCom, 5 models, ari only	-3.9 (-13.3 to -1.0)
		<i>This study</i>	ECLIPSE, 1 model, 3 source regions, 2 seasons, ari+aci	-0.5 to -1.4 depending on region
CH ₄	CH ₄	Stevenson et al. (2013)	ACCMIP, 6 models	+2.2 (+1.8 to +3.0)
		<i>This study</i>	ECLIPSE, 3 models	+1.5 (+1.2 to +2.0)
	O ₃	Stevenson et al. (2013)	ACCMIP, 6 models	+0.7 (+0.5 to +1.0)
		<i>This study</i>	ECLIPSE, 3 models	+0.5 (+0.4 to +0.7)
NO _x	CH ₄	Stevenson et al. (2013)	ACCMIP, 6 models	-5.5 (-7.4 to -4.2)
		<i>This study</i>	ECLIPSE, 3 models, includes primary-mode O ₃	-0.4 to -2.1 (-2.6 to -2.5) depending on region
	O ₃	Stevenson et al. (2013)	ACCMIP, 6 models	+1.9 (+1.7 to +3.3)
		<i>This study</i>	ECLIPSE, 3 models	+0.1 to +1.4 (+0.1 to +1.5) depending on region
	Aerosols	<i>This study</i>	ECLIPSE, 3 models, ari+aci	-0.3 to -0.8 (-1.2 to +0.2) depending on region
CO	CH ₄	Stevenson et al. (2013)	ACCMIP, 6 models	+0.11 (+0.07 to +0.13)
		<i>This study</i>	ECLIPSE, 3 models, includes primary-mode O ₃	+0.12 to +0.15 (+0.08 to +0.20) depending on region



	O ₃	Stevenson et al. (2013)	ACCMIP, 6 models	+0.11 (+0.08 to 0.14)
		<i>This study</i>	ECLIPSE, 3 models	+0.03 to +0.06 (+0.03 to +0.07) depending on region
	Aerosols	<i>This study</i>	ECLIPSE, 3 models, ari+aci	+0.02 to +0.05 (−0.01 to +0.12) depending on region
NMVOC	CH ₄	Stevenson et al. (2013)	ACCMIP, 6 models	+0.27 (+0.00 to +0.41)
		<i>This study</i>	ECLIPSE, 3 models, includes primary-mode O ₃	+0.35 to +0.66 (+0.02 to +0.93) depending on region
	O ₃	Stevenson et al. (2013)	ACCMIP, 6 models	+0.34 (+0.21 to +0.39)
		<i>This study</i>	ECLIPSE, 3 models	+0.63 to +1.15 (+0.31 to +1.48) depending on region
	Aerosols	<i>This study</i>	ECLIPSE, 3 models, ari+aci	−0.18 to −0.74 (−1.48 to +0.86) depending on region

1



1 **Table 2.** List of models participating in the ECLIPSE radiative forcing simulations. Models
 2 are either general circulation models (GCM) or chemistry-transport models (CTM).
 3 Resolution indicates the horizontal resolution, in degrees, and the number of vertical levels.
 4 Crosses indicate which aerosol species are represented in each model, among sulphate (SO₄),
 5 black carbon (BC), organic carbon (OC), secondary organic aerosol (SOA), and nitrate
 6 (NO₃) aerosols. Chemistry indicates whether the model includes an interactive tropospheric
 7 ozone chemistry scheme. Radiation indicates whether radiation calculations are done
 8 interactively (online) or offline from monthly distributions. Note that ozone radiative forcing
 9 calculations are done offline for all models.

Model	Type	Resolution	SO ₄	BC	OC	SOA	NO ₃	Chemistry	Radiation
ECHAM6- HAM2	GCM	1.8°x1.8° L31	X	X	X				Online
HadGEM3- GLOMAP	GCM	1.8°x1.2° L38	X	X	X	X		X	Online
NorESM1- M	GCM	1.9°x2.5° L26	X	X	X	X		X	Online
OsloCTM2	CTM	2.8°x2.8° L60	X	X	X	X	X	X	Offline

10



1 **Table 3.** List of simulations made to provide radiative forcing by regional and seasonal
 2 perturbations, and size of the emission perturbation applied to the anthropogenic component
 3 for the year 2008, in Tg yr^{-1} . For some ozone precursors, HadGEM3 also perturbed the
 4 biomass-burning component so the size of its perturbation is given in bracket (H:) for species
 5 and regions with strong biomass-burning sources. Emitted masses are in [C] for black and
 6 organic carbon, and volatile organic compounds. They are in $[\text{NO}_2]$ for NO_x .

#	Perturbation applied	Emission perturbation (Tg yr^{-1})	
		May—Oct	Nov—Apr
1	None (control simulation)		
2	SO_2 emissions reduced by 20% in Europe	-0.77	-0.85
3	SO_2 emissions reduced by 20% in East Asia	-3.14	-3.35
4	SO_2 emissions reduced by 20% outside Europe, East Asia, and shipping sector	-5.1	-5.2
5	BC emissions reduced by 20% in Europe	-0.03	-0.05
6	BC emissions reduced by 20% in East Asia	-0.11	-0.18
7	BC emissions reduced by 20% outside Europe, East Asia, and shipping sector	-0.35	-0.36
8	OC emissions reduced by 20% in Europe	-0.04	-0.07
9	OC emissions reduced by 20% in East Asia	-0.21	-0.37
10	OC emissions reduced by 20% outside Europe, East Asia, and shipping sector	-0.80	-0.83
11	NH_3 emissions reduced by 20% in Europe	-0.39	-0.39
12	NH_3 emissions reduced by 20% in East Asia	-1.37	-1.35
13	NH_3 emissions reduced by 20% outside Europe, East Asia, and shipping sector	-3.48	-3.43



14	NO _x emissions reduced by 20% in Europe	-1.00	-1.06
15	NO _x emissions reduced by 20% in East Asia	-2.03	-2.11
16	NO _x emissions reduced by 20% outside Europe, East Asia, and shipping sector	-6.27 (H: -7.17)	-6.37 (H: -6.69)
17	VOC emissions reduced by 20% in Europe	-0.06 to - 0.28	-0.07 to - 0.36
18	VOC emissions reduced by 20% in East Asia	-0.15 to - 0.55	-0.19 to - 0.84
19	VOC emissions reduced by 20% outside Europe, East Asia, and shipping sector	-0.15 to - 4.08	-0.19 to - 4.17
20	CO emissions reduced by 20% in Europe	-2.43	-3.09
21	CO emissions reduced by 20% in East Asia	-12.82 (H: -12.91)	-16.99 (H: -17.58)
22	CO emissions reduced by 20% outside Europe, East Asia, and shipping sector	-35.65 (H: -64.39)	-35.10 (H: -51.40)
23	All species of the shipping sector reduced by 20%	See Table 4.	
24	CH ₄ perturbations equivalent to global 20% emission reduction	See ΔE in Table 7.	

1



- 1 **Table 4.** Size of the emission perturbation applied to the shipping sector for the year 2008, in
 2 $Tg\ yr^{-1}$. Emitted masses are in [C] for black and organic carbon, and volatile organic
 3 compounds. They are in [NO₂] for NO_x. Emissions used in ECHAM6 and NorESM1 are
 4 denoted with E and N, where different.

Species	Emission perturbation ($Tg\ yr^{-1}$)	
	May—Oct	Nov—Apr
SO ₂	-1.04 (E: -1.25)	-1.04 (E: -1.24)
BC	-0.01 (E: -0.02)	-0.01 (E: -0.02)
OC	-0.01 (E: -0.02)	-0.01 (E: -0.02)
NO _x	-1.70 (N: -1.10)	-1.67 (N: -1.10)
VOC	-0.04 to -0.21	-0.04 to -0.21
CO	-0.11	-0.11

5
6



1 **Table 5.** *Simulated lifetime, in days, of aerosol species and tropospheric ozone in the four*
 2 *participating models.*

Species	ECHAM6	HadGEM3	NorESM1	OsloCTM2
Sulphate	4.0	5.2	4.2	3.5
BC	5.2	5.7	8.0	6.2
OC	5.0	6.6	7.7	5.0
Tropospheric ozone	n/a	20.7	26.4	Not diagnosed

3
4



1 **Table 6.** *Semi-direct radiative forcing (SDRF) by regional and seasonal perturbations of*
2 *black carbon aerosols. Column 3 gives the scaling factor imposed to let rapid adjustments*
3 *from the semi-direct effect emerge from natural variability. Column 4 gives the corresponding*
4 *specific SDRF, in $mW m^{-2} (Tg[C] yr^{-1})^{-1}$, and its standard deviation over the 30 years.*
5

Region	Season	Scaling factor	Specific SDRF
Europe	Summer	500	-31 ± 13
	Winter	500	-3 ± 8
East Asia	Summer	150	-38 ± 12
	Winter	150	$+1 \pm 7$
Global	Summer	30	-40 ± 18
	Winter	30	-14 ± 11

6

7



1 **Table 7.** Characteristics of the methane budget in ECLIPSE models. For NorESM1, numbers
 2 are given for the Summer perturbation simulation. From left to right, columns give: methane
 3 lifetime to destruction by OH, τ_{OH} in years, for the control (Ctl) and perturbed (Per)
 4 simulations; total methane lifetime, τ_{tot} in years, in Ctl and Per simulations; total methane
 5 burden, B in $Tg[CH_4]$, in Ctl and Per simulations; methane feedback factor f ; equivalent
 6 methane emission perturbation, ΔE in $Tg[CH_4] yr^{-1}$; methane radiative forcing, RF in
 7 $mW m^{-2}$; methane specific radiative forcing, SRF in $mW m^{-2} (Tg[CH_4] yr^{-1})^{-1}$. See Sect. 3.5 for
 8 details.

Model	τ_{OH}		τ_{tot}		B		f	ΔE	RF	SRF
	Ctl	Per	Ctl	Per	Ctl	Per				
HadGEM3	6.0	5.6	5.5	5.2	4561	3702	1.34	117	123	1.21
NorESM1	7.8	7.7	7.0	6.9	4815	4489	1.28	36.5	44	1.38
OsloCTM2	10.2	9.6	8.9	8.4	4909	4115	1.46	61	109	2.04

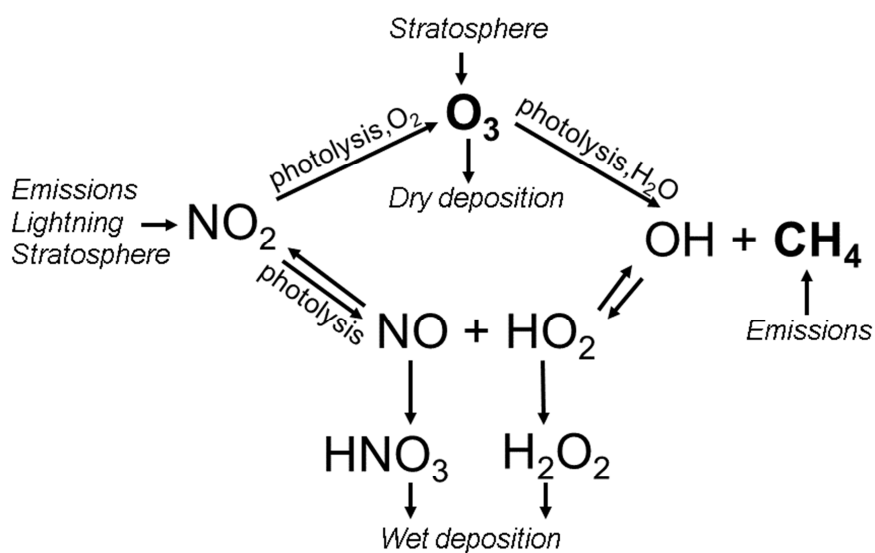
9



1 **7 Figures**

2

3 **Figure 1.** *Simplified description of tropospheric ozone chemistry. Arrows represent chemical*
4 *reactions and, for processes noted in italics, sources and sinks. For the sake of simplicity, the*
5 *role of volatile organic compounds is not shown, but discussed in the main text.*

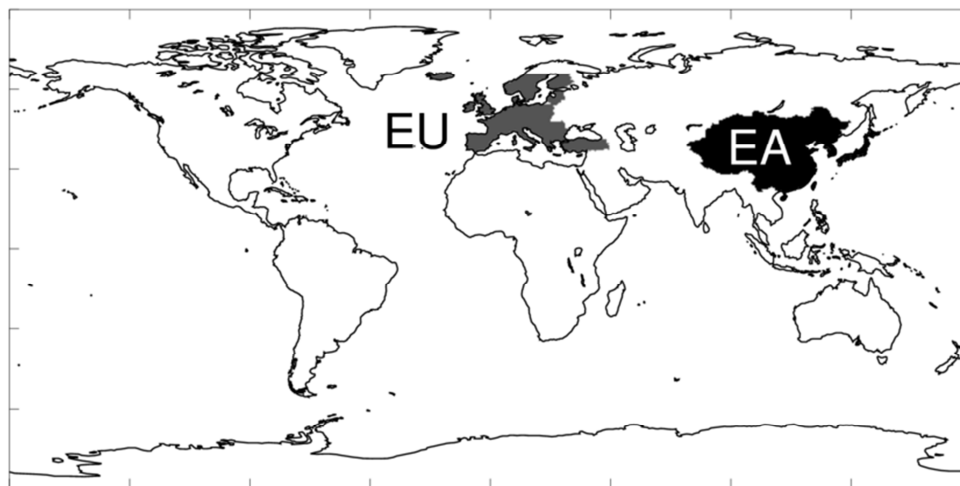


6

7



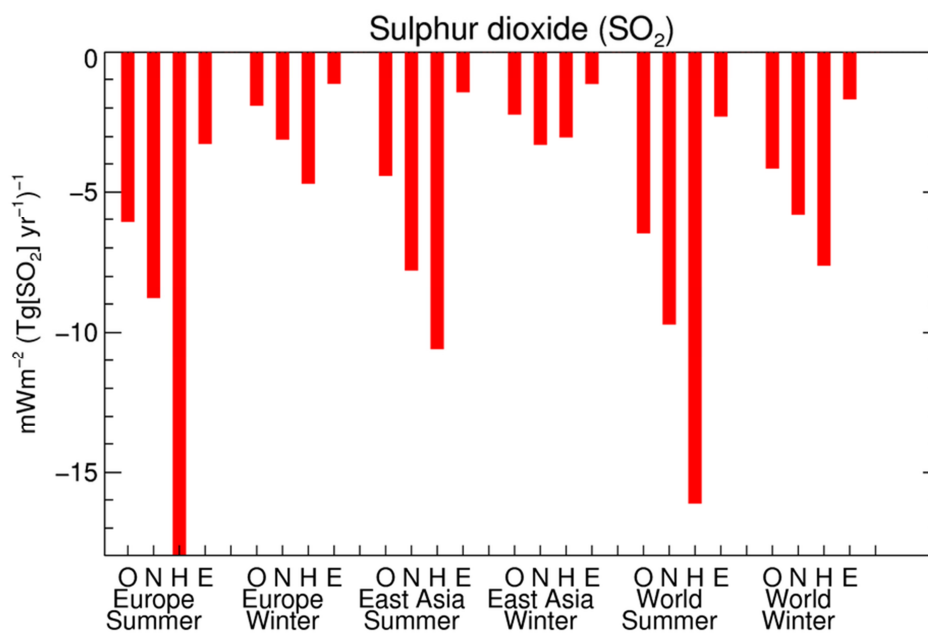
- 1 **Figure 2.** HTAP tier-1 regions used in the ECLIPSE specific radiative forcing matrix. EU
- 2 stands for Europe and EA for East Asia.



- 3
- 4



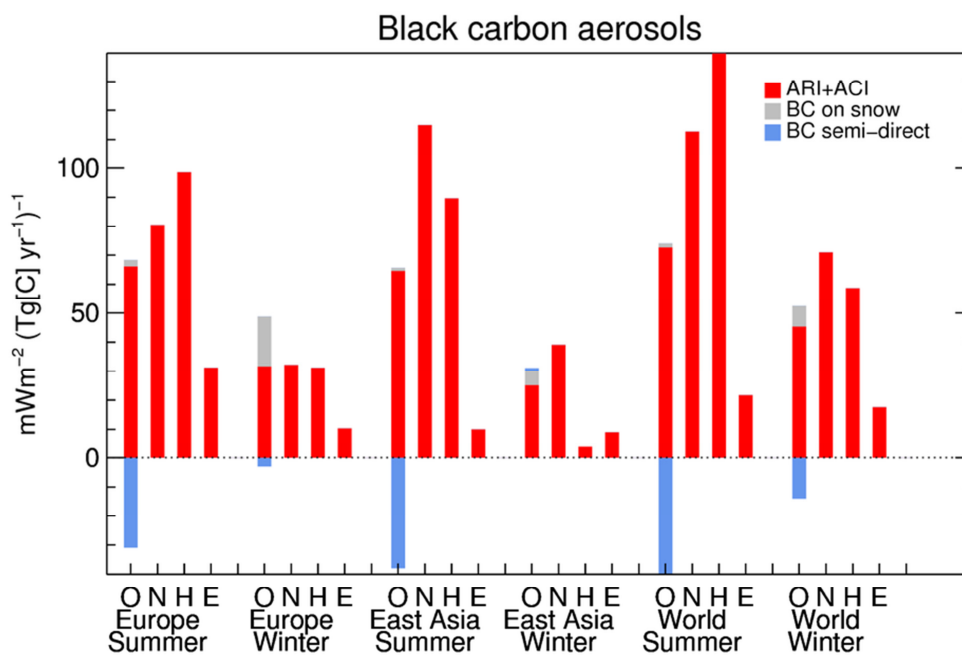
1 **Figure 3.** Specific radiative forcing, in $\text{mW m}^{-2} (\text{Tg}[\text{SO}_2] \text{ yr}^{-1})^{-1}$, for regional and seasonal
2 reductions in sulphur dioxide emissions. Results are obtained by four global models:
3 OsloCTM2 (O), NorESM1 (N), HadGEM3 (H), and ECHAM6 (E). Radiative forcing is
4 diagnosed as the sum of aerosol-radiation and aerosol-cloud interactions, except for
5 ECHAM6 which diagnoses aerosol-radiation interactions only.



6
7



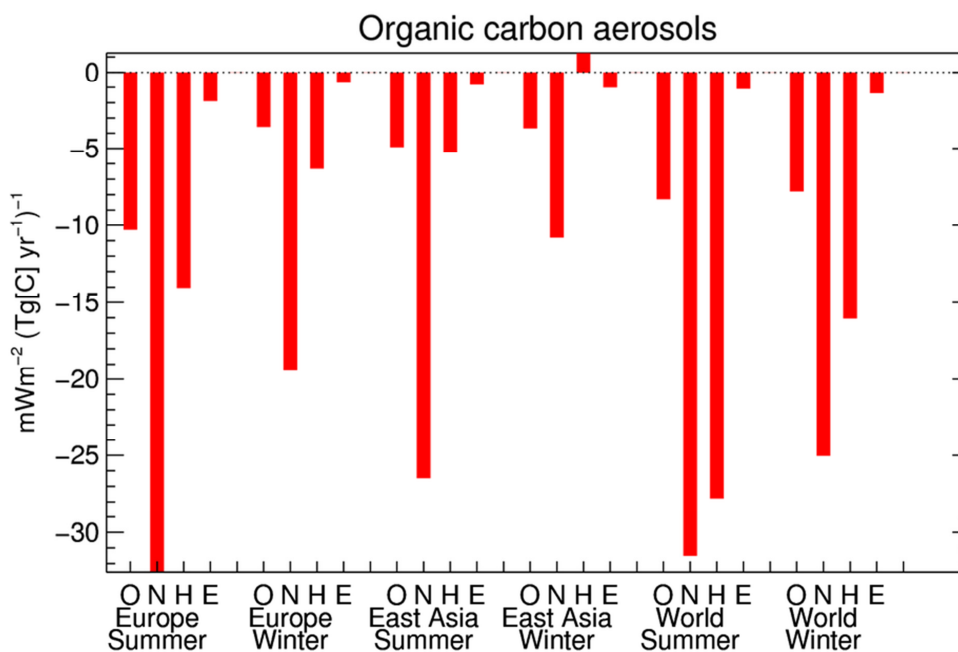
1 **Figure 4.** Specific radiative forcing, in $\text{mW m}^{-2} (\text{Tg}[C] \text{ yr}^{-1})^{-1}$, for regional and seasonal
 2 reductions in primary black carbon aerosol emissions. Results are obtained by four global
 3 models: OsloCTM2 (O), NorESM1 (N), HadGEM3 (H), and ECHAM6 (E). Three categories
 4 of radiative forcing mechanisms are included: aerosol-radiation and aerosol-cloud
 5 interactions (red, except for ECHAM6 where aerosol-cloud radiative forcing is not
 6 diagnosed), BC deposition on snow (grey, OsloCTM2 only), and rapid adjustments from the
 7 semi-direct effect of BC (blue, OsloCTM2 only).



8
 9



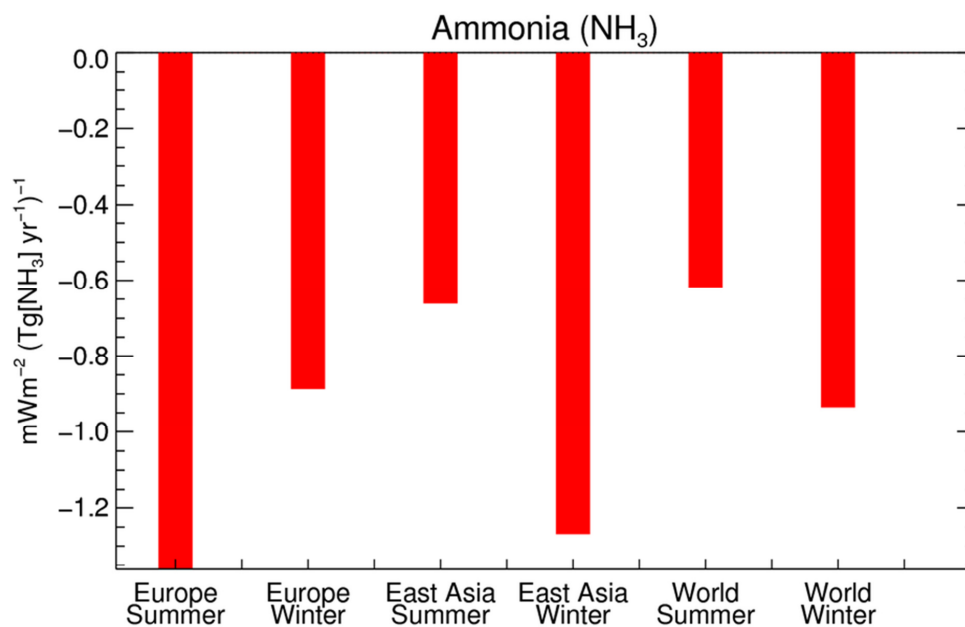
1 **Figure 5.** Specific radiative forcing, in $\text{mW m}^{-2} (\text{Tg}[C] \text{ yr}^{-1})^{-1}$, for regional and seasonal
2 reductions in primary organic carbon aerosol emissions. Results are obtained by four global
3 models: OsloCTM2 (O), NorESM1 (N), HadGEM3 (H), and ECHAM6 (E). Radiative forcing
4 is diagnosed as the sum of aerosol-radiation and aerosol-cloud interactions, except for
5 ECHAM6 which diagnoses aerosol-radiation interactions only.



6
7



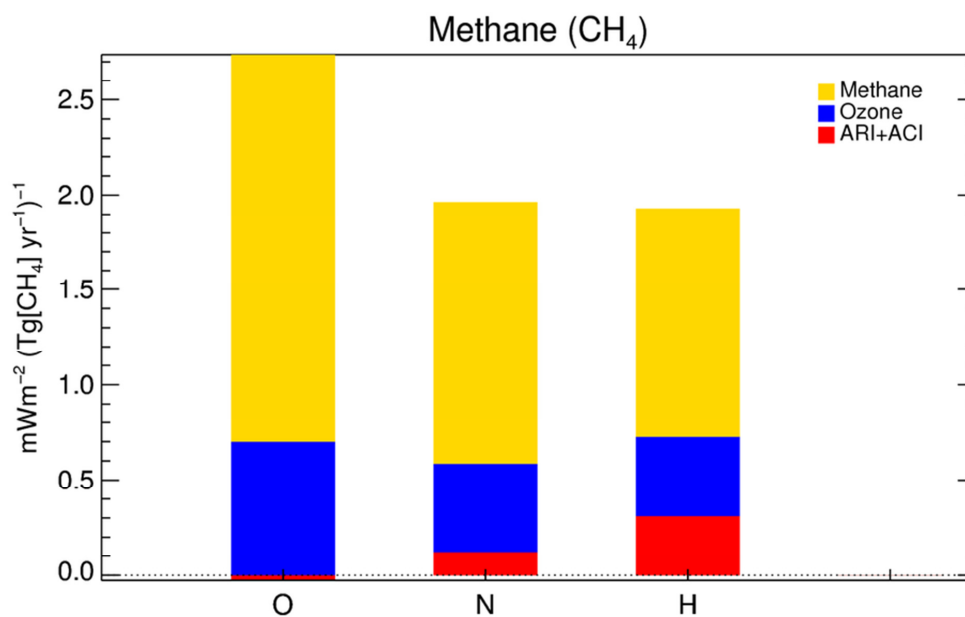
- 1 **Figure 6.** Specific radiative forcing, in $\text{mW m}^{-2} (\text{Tg}[\text{NH}_3] \text{ yr}^{-1})^{-1}$, for regional and seasonal
- 2 reductions in ammonia emissions. Results are obtained by the OsloCTM2 model, and include
- 3 aerosol-radiation and aerosol-cloud interactions.



4
5



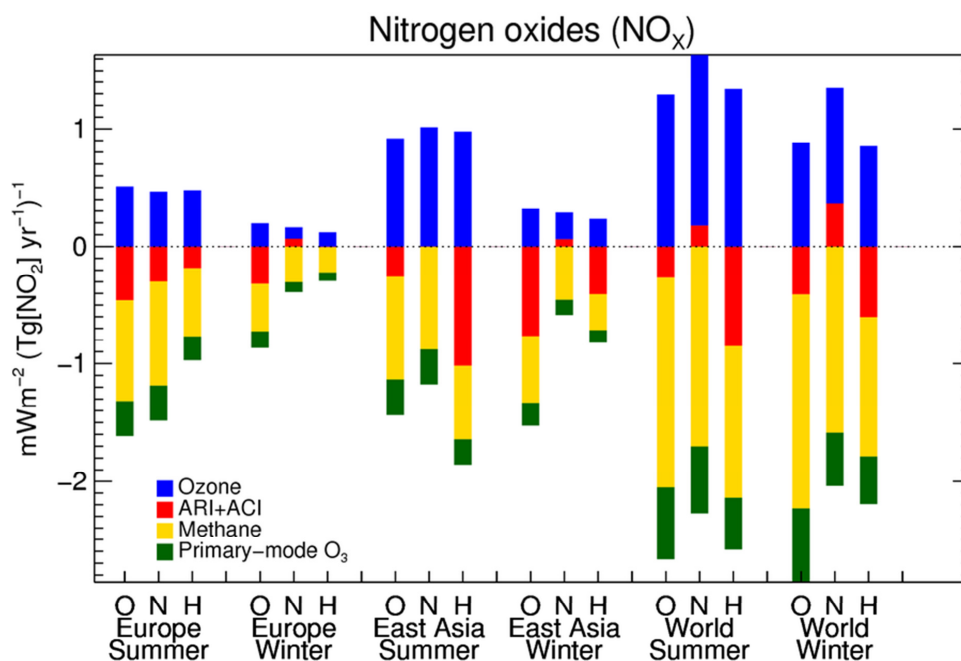
1 **Figure 7.** Specific radiative forcing, in $\text{mW m}^{-2} (\text{Tg}[\text{CH}_4] \text{ yr}^{-1})^{-1}$, for global and annual
2 reductions in equivalent methane emissions (see Sect. 3.5 for details). Results are obtained by
3 three global models: OsloCTM2 (O), NorESM1 (N), and HadGEM3 (H). Three categories of
4 radiative forcing mechanisms are included: aerosol-radiation and aerosol-cloud interactions
5 (red), short-term changes in ozone (blue), and methane (yellow).



6
7



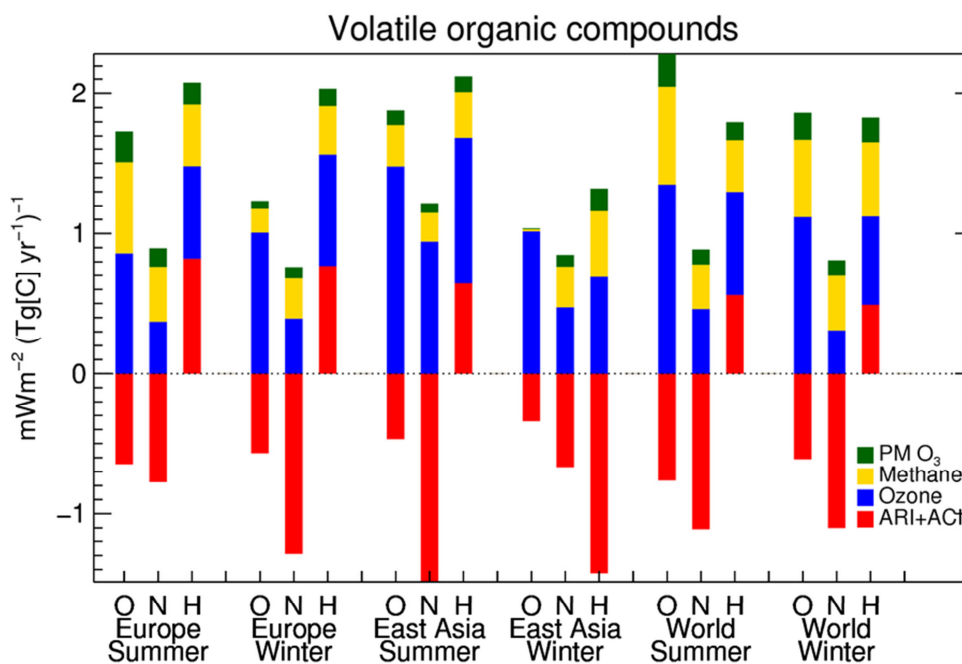
1 **Figure 8.** Specific radiative forcing, in $\text{mW m}^{-2} (\text{Tg}[\text{NO}_2] \text{ yr}^{-1})^{-1}$, for regional and seasonal
 2 reductions in nitrogen oxide emissions. Results are obtained by three global models:
 3 OsloCTM2 (O), NorESM1 (N), and HadGEM3 (H). Four categories of radiative forcing
 4 mechanisms are included: aerosol-radiation and aerosol-cloud interactions (red), short-term
 5 changes in ozone (blue), methane (yellow), and primary-mode ozone (green).



6
 7



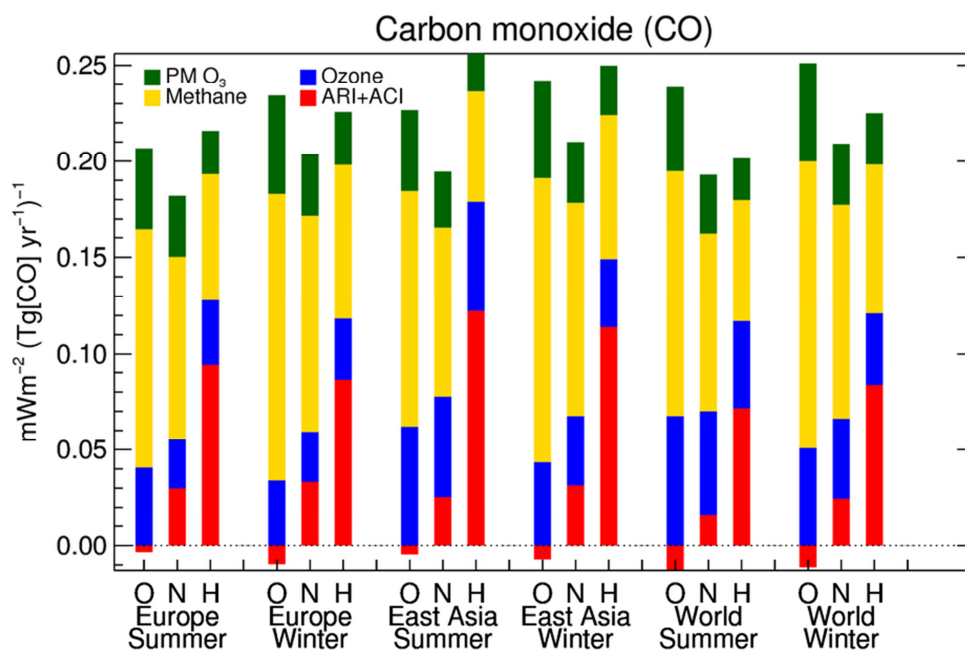
1 **Figure 9.** Specific radiative forcing, in $\text{mW m}^{-2} (\text{Tg}[C] \text{ yr}^{-1})^{-1}$, for regional and seasonal
2 reductions in emissions of volatile organic compounds. Results are obtained by three global
3 models: OsloCTM2 (O), NorESM1 (N), and HadGEM3 (H). Four categories of radiative
4 forcing mechanisms are included: aerosol-radiation and aerosol-cloud interactions (red),
5 short-term changes in ozone (blue), methane (yellow), and primary-mode ozone (green).



6
7



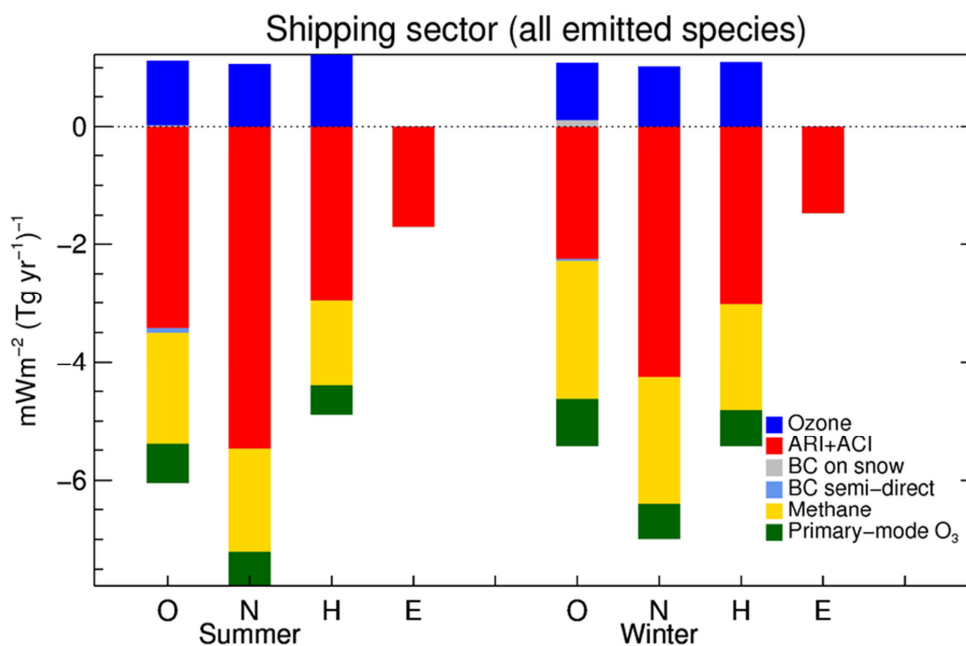
1 **Figure 10.** Specific radiative forcing, in $\text{mW m}^{-2} (\text{Tg}[\text{CO}] \text{ yr}^{-1})^{-1}$, for regional and seasonal
 2 reductions in emissions of carbon monoxide. Results are obtained by three global models:
 3 OsloCTM2 (O), NorESM1 (N), and HadGEM3 (H). Four categories of radiative forcing
 4 mechanisms are included: aerosol-radiation and aerosol-cloud interactions (red), short-term
 5 changes in ozone (blue), methane (yellow), and primary-mode ozone (green).



6
7



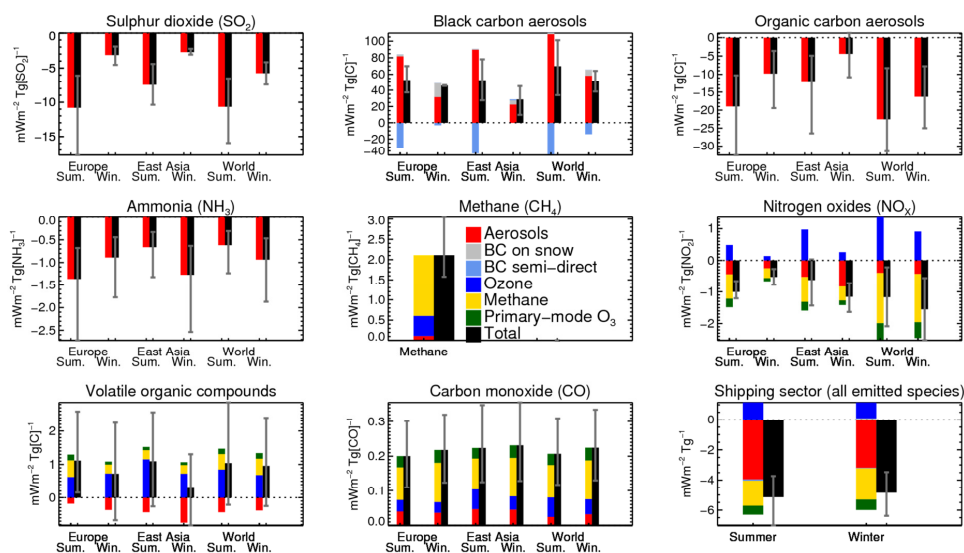
1 **Figure 11.** Specific radiative forcing, in $\text{mW m}^{-2} (\text{Tg yr}^{-1})^{-1}$, for seasonal reductions in all the
 2 species emitted by the shipping sector. The species included and their units of emitted mass
 3 are sulphur dioxide (SO_2), black carbon (C), organic carbon (C), ammonia (NH_3), nitrogen
 4 oxides (NO_2), volatile organic compounds (C), carbon monoxide (CO), and methane (CH_4).
 5 Results are obtained by four global models: OsloCTM2 (O), NorESM1 (N), HadGEM3 (H),
 6 and ECHAM6 (E). Six categories of radiative forcing mechanisms are included: aerosol-
 7 radiation and aerosol-cloud interactions (red, except for ECHAM6 which diagnoses aerosol-
 8 radiation only), black carbon deposition on snow (grey, OsloCTM2 only), black carbon rapid
 9 adjustments from the semi-direct effect (light blue, OsloCTM2 only), short-term changes in
 10 ozone (dark blue, not simulated by ECHAM6), methane (yellow, not simulated by ECHAM6),
 11 and primary-mode ozone (green, not simulated by ECHAM6).



12
 13



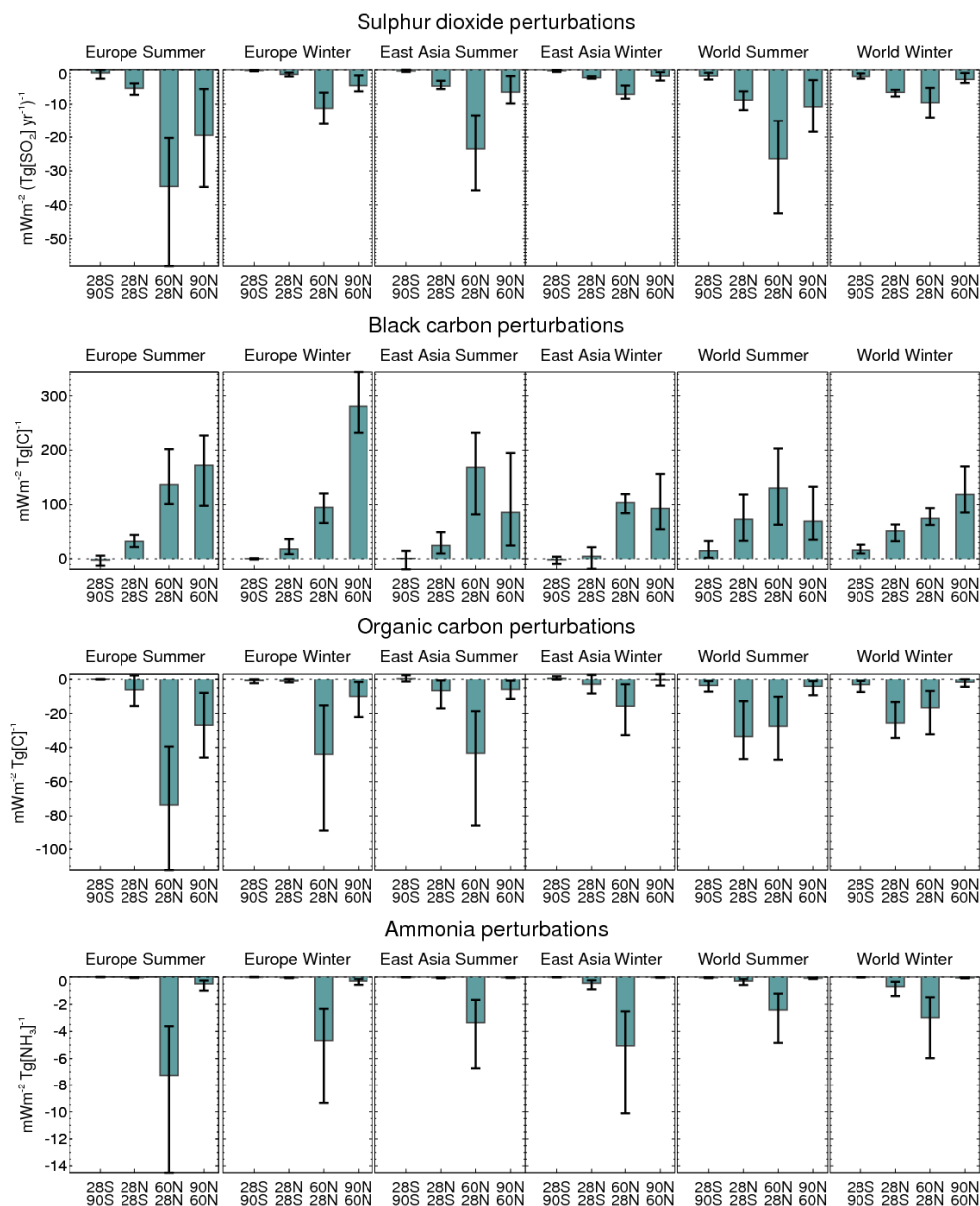
1
2 **Figure 12.** Best estimates of specific radiative forcing for regional and seasonal reductions in
3 near-term climate forcer emissions, in $\text{mW m}^{-2} (\text{Tg yr}^{-1})^{-1}$. Best estimates are given for six
4 categories of radiative forcing: aerosol-radiation and aerosol-cloud interactions (red), black
5 carbon deposition on snow (grey), black carbon rapid adjustments from semi-direct effects
6 (light blue), short-term changes in ozone (dark blue), methane (yellow), and primary-mode
7 ozone (green). Black bars show the total specific radiative forcing, i.e. the sum of the six
8 components listed above, and whiskers denote the weakest and strongest specific radiative
9 forcing that are obtained by the four participating models or, in the case of ammonia
10 perturbations, estimated from the literature.



11
12



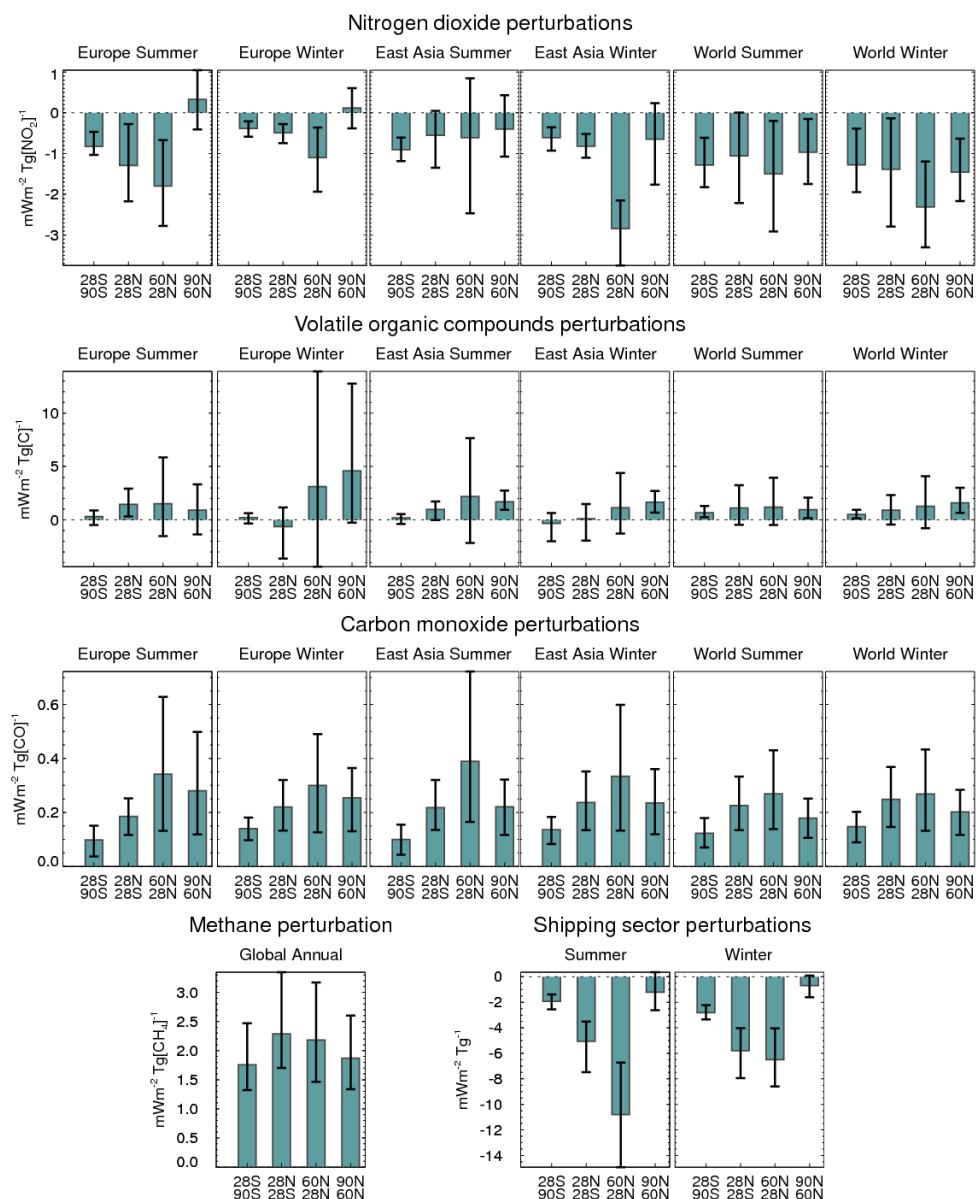
1 **Figure 13a.** Best estimates of annually-averaged specific radiative forcing, in mW m^{-2}
 2 $(\text{Tg}[\text{species}] \text{ yr}^{-1})^{-1}$, in four latitude bands, for aerosol primary and precursor emission
 3 perturbations. Each row corresponds to a perturbed species: from top to bottom, sulphur
 4 dioxide, black carbon, organic carbon, and ammonia. Each column corresponds to a regional
 5 and seasonal perturbation. Barcharts are shown for four latitude bands, from left to right:
 6 90N–60N, 60N–28N, 28N–28S, and 28S–90S.
 7



8



1 **Figure 13b.** As Figure 13a, but for ozone precursor and shipping sector perturbations.
 2 Perturbed species are, from top to bottom, nitrogen oxide, volatile organic compounds,
 3 carbon monoxide, methane, and all species emitted by the shipping sector.
 4



5
 6